Journal of Asian Earth Sciences 147 (2017) 284–309

Contents lists available at ScienceDirect

Journal of Asian Earth Sciences

journal homepage: www.elsevier.com/locate/jseaes

Full length article

The arcuate fold-and-thrust belt of northern Taiwan: Results of a two-stage rotation revealed from a paleomagnetic study

Lionel Sonnette[a,*], Jian-Cheng Lee[b], Chorng-Shern Horng[b]

[a] UMR SPE CNRS 6134, Laboratoire d'Hydrogéologie, Campus Grimaldi, 20250 Corte, France
[b] Institute of Earth Sciences, Academia Sinica, 128 Academia Road, Section 2, Taipei 115, Taiwan

ARTICLE INFO

Keywords:
Salient
Fold-and-thrust belt
Rotation
Paleomagnetism
North Taiwan

ABSTRACT

The Taiwan orogen is the result of the collision of the Luzon Volcanic Arc pushed northwestward by the Philippine Sea Plate against the Chinese Continental Margin since the Late Miocene and is still uplifting nowadays. The fold-and-thrust belt in northern Taiwan shows an arcuate shape from SW to NE: the strike of the main tectonic structures changes from N0°E to N70°E. Such curvature has not yet been properly interpreted so far. In this study we used paleomagnetic analyses to decipher the tectonic evolution along the fold-and-thrust belt in northern Taiwan, which reveals complex magnetization patterns both in ante-folding and post-folding formations. We also interpret that the fold-and-thrust belt in northern Taiwan has experienced two main rotational events: a 30–60 ± 14° clockwise rotation followed by a 30 ± 7° counterclockwise rotation during the ages of 4.6–1.5 Ma.

1. Introduction

The Taiwan mountain range in its northern half presents increasing magnitudes of curvatures in map viewed from south towards north and from foreland towards hinterland (Fig. 1). From south to north, the trend of the major geological structures deviates clockwise from N0°E to N70°E in the Western Foothills and the Hsuehshan Range, and from N0°E to N100°E in the Central Range. Such bending curvatures for a fold-and-thrust belt within a mountain range have captured scientist attention worldwide for a long time (Carey, 1955; Marshak, 2004; Weil and Sussman, 2004). A mountain belt with a convex shape is commonly called a salient (Miser, 1932). Thus the term North Taiwan Foreland Salient (NTFS) is used in this paper. The geometry of a salient is generally quite evident to observe, however, its evolution is difficult to describe. The study of paleomagnetism that analyzes the remanent magnetization of rocks has the ability to determine horizontal block rotation and to provide relative chronology with respect to folding/tilting of the strata in orogens around the world (Weil and Sussman, 2004; Van der Voo, 2004; Pueyo et al., 2016).

The Taiwan Island is an emerged manifestation of mountain building under complex geodynamical contexts (Fig. 1). It relates to a collision between the Luzon Volcanic Arc and the Chinese Continental Margin (Biq, 1972; Covey, 1984; Suppe, 1984; Malavieille et al., 2002), an extension of the Okinawa Trough (Sibuet et al., 1987; Shinjo and Kato, 2000; Lallemand, 2014), and a flip of polarity between two opposing subduction zones (Suppe, 1984; Chemenda et al., 1997; Teng et al., 2000). The Taiwan mountain range itself has undergone significant deformation, produced by multiple geological processes, including thrusting, folding, bending, shortening, shearing, exhumation, and so on. Although many studies have discussed about the curved shape of the NTFS (Juan, 1975; Suppe, 1984; Macedo and Marshak, 1999; Clift et al., 2008; Mirakian et al., 2013), they only provided hypothesis about its origin. By far only a few studies are supported by paleomagnetic data (Hsu et al., 1966; Lee et al., 1991; Miki et al., 1993; Lue et al., 1995). However these paleomagnetic studies only covered one third of the whole NTFS (Fig. 1) and their interpretations are inconsistent with each other (see Section 2.3). Consequently, the amounts and the timing of rotation in the NTFS remain uncertain and questionable.

Here we present new paleomagnetic data and analyses in the NTFS in order to fill the gap with the previous studies. Our main purpose is to characterize the rotational pattern of the NTFS. Our results allow establishing its tectonic history by evoking two episodes of regional block rotations. In the end of this paper, we propose a trigonometric model to restore the shortening trajectories of the NTFS during the collision and mountain building. We also discuss the respective contributions of the arc-continent collision and of the opening of the Okinawa Trough to the horizontal block rotations in the NTFS.

* Corresponding author.
E-mail address: lsonnette@gmail.com (L. Sonnette).

http://dx.doi.org/10.1016/j.jseaes.2017.07.026
Received 24 February 2017; Received in revised form 11 July 2017; Accepted 16 July 2017
Available online 19 July 2017

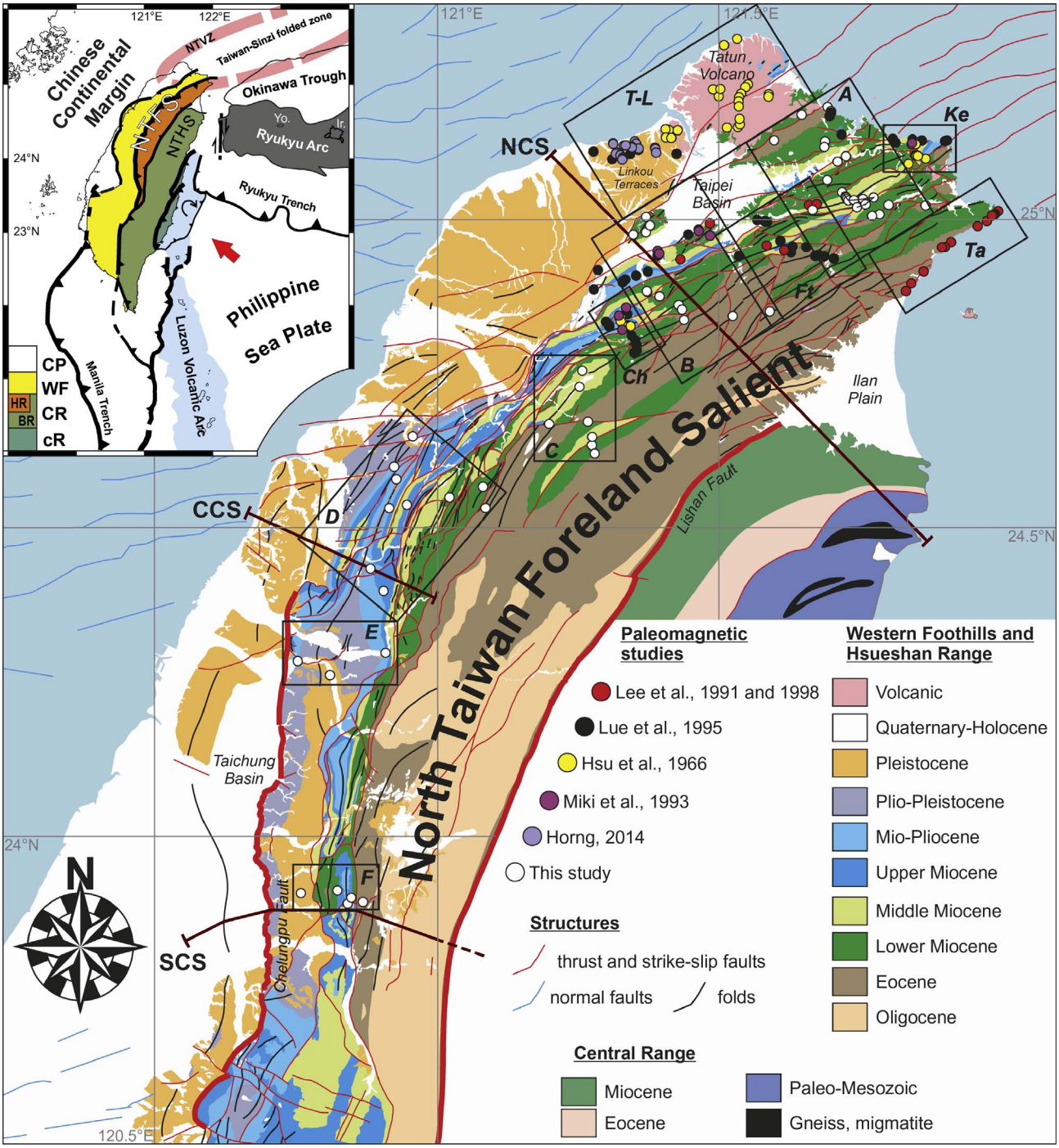

Fig. 1. Taiwan geodynamical map and geological map of the North Taiwan Foreland Salient with location of the sampling sites. Yo.: Yonaguni Island; Ir.: Iriomote Island; CP: Coastal Plain; WF: Western Foothills; CR: Central Range; HR: Hsuehshan Range; BR: Backbone Range; cR: Coastal Range; NTVZ: North Taiwan Volcanic Zone; NTFS: North Taiwan Foreland Salient; NTHS: North Taiwan Hinterland Salient; A-B-C-D-E-F: sampled area of this study; Ch: Chiaopanshan area; Ft: Fei-tsui reservoir area; T-L: Tatun-Linkou area; Ke: Keelung volcano group area; Ta: Tali coast area. The cross-sections mentionned in the text are mapped and labelled NCS, CCS and SCS for North, Central and South cross-section respectively.

2. Geological settings

2.1. General geology of Taiwan

As one of the most active and youngest mountain belts, Taiwan is the product of convergence of the Philippine Sea Plate (PSP) against the Chinese Continental Margin (CCM), which started 5 or 6 million years ago (Chai, 1972; Suppe, 1984; Teng, 1990; Huang et al., 1997). The current convergent rate has been estimated to be 8.2 cm/yr in the N306°E direction according to GPS measurements (Yu et al., 1997; Hsu et al., 2009). The plate convergence direction can be inferred to be oriented N335°E from ductile microstructure analyses in the Central metamorphic belt (Faure et al., 1991). The difference of 70° of original trends between the northern Luzon Arc (N10°W) and the Chinese Continental Margin (N64°E) indicates an oblique arc-continent collision. Because of this inherited geometry, the Luzon Volcanic Arc of the PSP acts as an indenter colliding into the CCM in the Northern Taiwan and the deformation has been propagating southward since then (Suppe, 1984; Lu et al., 1995; Byrne, 1998; Simoes and Avouac, 2006; Nagel et al., 2013).

The Taiwan Island is composed of four tectonostratigraphic units, from east to west: the Coastal Range, the Central Range, the Western Foothills and the Coastal Plain (Ho, 1986, Fig. 1). The Coastal Range is the northern extension of the Luzon Volcanic Arc accreted to the Central Range along the Longitudinal Valley (Biq, 1972; Bowin et al., 1978). The Central Range that is subdivided into the Hsueshan Range and the Backbone Range by the Lishan Fault is composed of deformed Permian to Miocene metamorphic rocks. These rocks recorded complex events including a Mesozoic plate subduction and a Cenozoic sediment burial and exhumation (Simoes et al., 2012) It was proposed that during its exhumation, the Backbone Range, bounded to the west by the Lishan Fault, plays as a deformable indenter in the setting up of the Hsuehshan Range, the Western Foothills and the Coastal Plain (e.g., Lu and Malavieille, 1994). The Western Foothills representing an ancient foreland basin is composed mainly of Oligocene to Pleistocene sedimentary rocks with volcanic rocks distributed in some local areas. The Coastal Plain is the present day foreland basin filled by shallow marine (e.g. deltaic) and non-marine (e.g., braided rivers) sand-dominated deposits (Nagel et al., 2013).

To the NE offshore of Taiwan, the Okinawa Trough represents the back-arc basin of the Ryukyu Arc to the South and is bounded by the Taiwan-Sinzi folded zone to the North (Wageman et al., 1970, Fig. 1). The Ryukyu Arc is the surface manifestation of the northward subduction of the PSP. Some metamorphic rocks distributed in the Ryukyu Islands (i.e. the Yonaguni and Iriomote) have compositions similar to that of the Central Range (Yoshiwara, 1901; Juan, 1975; Faure et al., 1988) and are separated from Taiwan by a major tear fault (Lallemand et al., 1997; Lallemand and Liu, 1998). The volcanic activities associated with the subduction of the PSP occurred mainly in the North of the Ryukyu Arc starting at about 18 Ma (Kizaki, 1986; Shinjo et al., 1999), whereas only small-scale activities appeared in the South near the Yonaguni Island (Lallemand and Liu, 1997). Another subduction-related magmatism in the western part of southern Ryukyu is the Northern Taiwan Volcanic Zone (NTVZ) with ages ranging from 2.8 to 0.4 Ma (Wang et al., 1999). Because of the opening of the Okinawa Trough, the Ryukyu Arc is now moving southward at a rate of 7 cm/yr relative to CCM and has a 25° clockwise rotation in the last 10 Myrs (Miki et al., 1990; Miki, 1995; Nakamura, 2004). Accompanying with this is the subduction of the PSP under the CCM propagating southwestward, which has resulted in changes of the crust of the northern Taiwan from shortening to extension since about 2 Ma (Bowin et al., 1978; Lee and Wang, 1988; Suppe, 1984; Lallemand et al., 2001). Such crustal extension was first interpreted as a manifestation of post-collisional collapse (Teng and Lee, 1996) which seems to be rather the result of a slab rollback (Ustaszewski et al., 2012).

2.2. Stratigraphy, structure and tectonics of the NTFS

The NTFS consists of the Western Foothills and the Hsuehshan Range (Fig. 1). Within these two units, different sediment supplies were recognized based on paleocurrents (Chou, 1973; Hong, 1988; Nagel et al., 2013). Initially the sediments were derived from the Chinese continental margin during the ages from the Oligocene to the latest Miocene, forming the oldest sedimentary package in the whole Hsueshan Range and the lowest part of the Western Foothills. They are typically shallow marine, near-shore deposits which filled a Paleogene half-graben basin bounded to the east by the west-dipping Lishan fault (Teng et al., 1991; Lee et al., 1997, Fig. 1). Along with the development of the Taiwan orogen during the Plio-Pleistocene, sediments sourced from Taiwan increased progressively compared to those from the Chinese margin. As a result, the Pleistocene formations in the Western Foothills are molasses supplied exclusively by the erosion of the uplifting Taiwan orogen (Lu and Hsu, 1992).

The sedimentary units forming the NTFS are imbricated through folding and thrusting processes (Suppe, 1981, 1983). It was estimated that along a main decollement located at the surface below the thick quartzite layer of the Oligocene Wuchishan formation (Elishewitz, 1963; Biq, 1966; Namson, 1984), the horizontal shortening at the north of the NTFS is in the range of 60–90 km (Suppe, 1986, NCS in Fig. 1), and is about 20–30 km both at the hinge of the NTFS (Hung and Wiltschko, 1993, CCS in Fig. 1) and at the south (Yue et al., 2005, SCS in Fig. 1). Coal layers in the Miocene formations acted as secondary slip/thrusting surfaces controlling the formation of imbricated systems (Suppe, 1980).

The present-day tectonic regime across the entire Taiwan Island is dominated by NW-SE trending compression revealed from stress inversions of fault slip measurements (Angelier et al., 1986), earthquake focal mechanism analyses (Yeh et al., 1991), and GPS strain observations (Hsu et al., 2009). However, the past tectonic history of the NTFS in terms of stress regime is rather complex and can be summarized as following. During the interval from the Oligocene to the late Miocene, N-S and NW-SE extensions prevailed (Angelier et al., 1990a; Teng et al., 1991; Lee et al., 1997; Hsiao et al., 1999). Then since about 6 Ma, up to 4 compression episodes in different directions have occurred, from old to young: N0°E (5–4 Ma), N67°E (4–3 Ma), N111°E (3–2 Ma), and N130°E-N155°E (<2 Ma) (Angelier et al., 1990b). Finally, extension occurred again in the northern part of the NTFS (Lee and Wang, 1988; Lee et al., 1997; Hu et al., 2002).

2.3. Previous paleomagnetic results in the NTFS

Hsu et al. (1966) first investigated paleomagnetic records of three

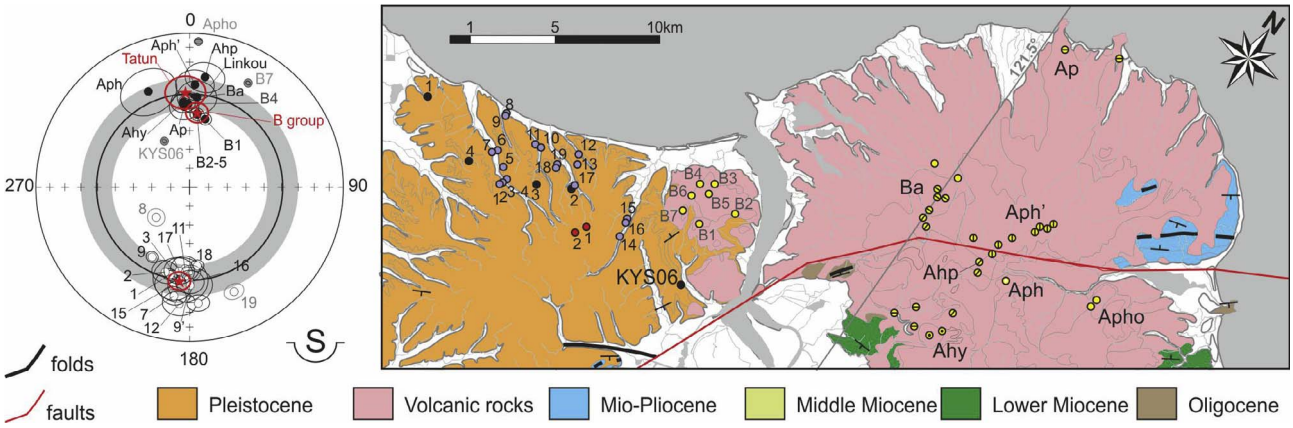

Fig. 2. Location of the sites and result of the study of Hsu et al. (1966) for the Tatun Volcano and of Horng (2014) for the Linkou area. In the stereographic projection the components of magnetization are presented *in situ* for the Linkou area because the dip of the bedding is less than 10°. The expected inclination for 0–40 Ma are represented by the grey circle, see Fig. 10 for more details.

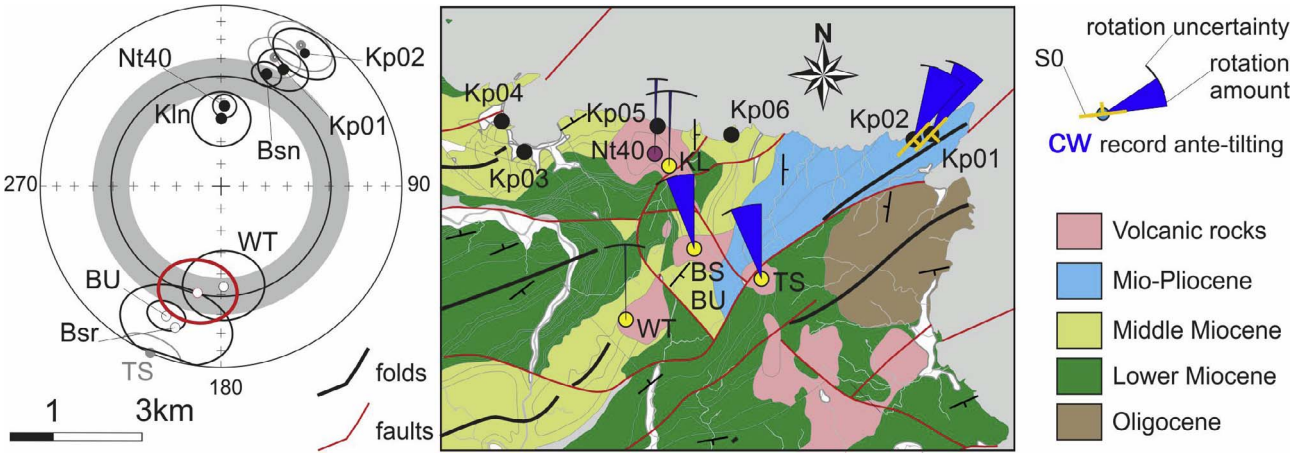

Fig. 3. Location of the sites and result of the study of Hsu et al. (1966) and Lue et al. (1995) for the Keelung Volcano. The expected inclination for 0–40 Ma are represented by the grey circle.

volcanic areas in the northern Taiwan: the Tatun Volcano Group (T-L area in Figs. 1 and 2), the Keelung Volcano Group (Ke area in Figs. 1 and 3) and the Chiaopanshan Area (Ch area in Fig. 1), which have respective ages of 1.5–0.2 Ma, 1.1 Ma, and 10–8 Ma (Wang et al., 2004). After discarding specimens that either show instability of remanent magnetizations during measurements or have large deviation of directions from those of other specimens within sites, they adopted 307 of 615 specimens for their final interpretation. Site-mean directions of stable remanent magnetizations indicate that the Tatun Volcano Group and the Chiaopanshan Area have no significant rotations, whereas the Keelung Volcano group has a 15° clockwise rotation, although paleomagnetic directions between sites are rather scattering probably due to locally tectonic effects, hydrothermal alterations, or geomagnetic secular variations.

Later, Miki et al. (1993) also used 8 of 13 paleomagnetic sites from the Keelung Volcano Group, the Chiaopanshan Area, and the early Miocene (ca. 20 Ma) Kungkuan volcanics in southwestern Taipei Basin (B area in Fig. 1) to interpret the tectonic history of northern Taiwan. Their paleomagnetic results are in agreement with those of Hsu et al. (1966), and concluded that no tectonic movement has occurred in northern Taiwan since 20 Ma.

On the other hand, Lee et al. (1991, 1998) and Lue et al. (1995) investigated the sedimentary and slightly metamorphosed packages of the NTFS from the Chiaopanshan area to the northeastern coast (Ch, B, Ft, A, Ta and Ke areas in Fig. 1), covering the ages from the Oligocene to the Pleistocene. They used 35 of 230 (Lee et al., 1991), 283 of 700 (Lue et al., 1995), 111 of 140 (Lee et al., 1998) specimens for their final interpretations. Based on their results, they proposed a post-Pliocene 20° counterclockwise rotation and a 15–50° clockwise rotation to the west and to the east of the Taipei basin, respectively.

More recently, Horng (2014) investigated magnetostratigraphy and calcareous nannofossil biostratigraphy of the sedimentary flat-lying Tananwan formation in the Linkou Tableland (T-L area in Fig. 1) to determine the age of the formation. The results indicate that the formation was deposited within the ages of 1.46–1.24 Ma, and no significant rotation was observed from the sampling sites.

In summary, there exist inconsistent interpretations for the tectonic movement of the NTFS between the studies of Miki et al. (1993), Lee et al. (1991) and Lue et al. (1995). Considering the complex tectonic structures in northern Taiwan, we regard that only a few volcanic sites that were analyzed in the study of Miki et al. (1993) is insufficient to decipher the tectonic evolution of the NTFS. In addition, according to petrographic observation and microprobe analysis of Yang (1986), the early Miocene Kungkuan volcanic rocks have already undergone deuteric alteration and different degrees of spilitization. Therefore, interpretation of the remanent magnetizations recorded in such rocks should be cautious. In fact, as shown in Section 4.3.7, the Chiaopanshan area has a complex rotational pattern, after considering all the results from Hsu et al. (1966, 1993) and Lue et al. (1995). The misleading of the interpretation of Lue et al. (1995) is first due to insufficient sampling. Their interpretations of clockwise and counterclockwise rotations on each side of the Taipei Basin are not exclusive. Statistically their interpretation requires to exclude some sites. Second, they did not explain how different sense of rotation on either side of the Taipei Basin can occur whereas the regional trend of the folds and thrust units remains continuous. Finally, the remanent magnetizations were interpreted or assumed to be recorded before folding or tilting of the strata. No proper stepwise unfolding (McFadden and Jones, 1981) or path unfolding analysis (Shipunov, 1997) had been conducted.

3. Sampling and laboratory analyses

In this study, we sampled 59 sites including 48 from the Western Foothills and 11 from the Hsuehshan Range (A22, A24, B9, B10, B11, C4, C5, C6, C7, D10 and F5), covering almost the whole stratigraphic sequence of the NTFS (Figs. 1B and 4, and Table 1). Most of sites were obtained from muddy layers intercalated with sandstones or from thick shaly layers, but a few were from massive sandstones. For each site an average of 11 paleomagnetic cores (25 mm in diameter) and a total of 653 cores were collected using an electric drill cooled with water and then oriented using a mechanical device with a compass and an inclinometer. The bedding planes of strata were measured for tilt correction and fold test. For the sites in the Hsueshan Range, schistosity (i.e., slaty cleavage) is often mixed up with and sub-parallel to the bedding plane.

The oriented cores were cut into standard specimens (22 mm in length) for paleomagnetic and rock magnetic analyses conducted at the Institute of Earth Sciences, Academia Sinica in Taipei. Several methods were performed to characterize magnetic concentration, grain size and composition of samples. As a proxy of magnetic concentration, low-field magnetic susceptibility (K_m) was measured on each specimen using an AGICO KLY-3 Kappabridge. Hysteresis loops and remanent curves were measured using a Lake Shore Cryotronics vibrating sample magnetometer (MicroMag^{TM}Model 3900). Magnetic fields from +0.5 T to −0.5 T were applied either to rock fragments retrieved during the core cutting or to magnetic extracts separated from collected samples. Saturation magnetization (M_s), remanent saturation magnetization (M_{rs}), and coercive force (H_c) were then determined after high-field slope correction for paramagnetic contribution. The remanent coercive force (H_{cr}) was determined by applying increasing back-fields after saturation at −0.5 T. The ratios of M_{rs}/M_s and H_{cr}/H_c were then plotted in a Day figure to evaluate the distribution of magnetic grain size (Day

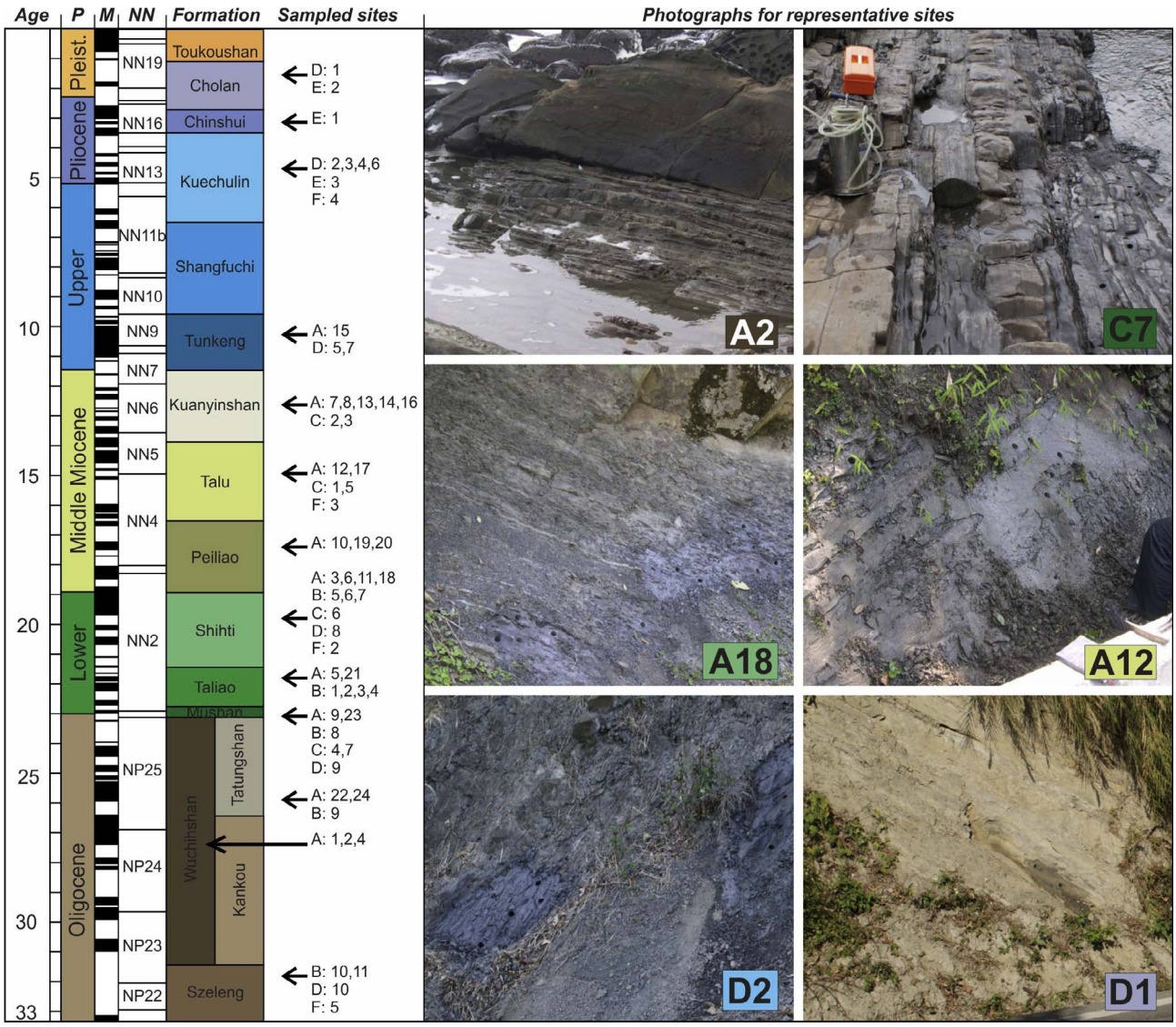

Fig. 4. Schematic stratigraphic log of the studied area and related sampled sites (A2, A12, A18 and C7: muddy layers intercalated with sandstones; D2: thick shaly layers; D1: massive sandstones). Age: absolute age (Ma); P.: period; G.: geomagnetic polarity; NN.: zonations of calcareous nannofossils. This time scale had been partly done with Time Scale Creator 6.3 software based on the Geologic Time Scale 2012 (Gradstein et al., 2012).

et al., 1977). To understand magnetic composition in the specimens, we followed the Lowrie method (Lowrie, 1990). Fields of 2 T, 0.5 T, and 0.1 T were applied to the three different axes of the specimens using a Magnetic Measurements pulse magnetizer to acquire a composite of remanent magnetizations. The specimens were then demagnetized stepwise from room temperature to 700 °C using a Sogo thermal demagnetizer (Zheng et al., 2010). To monitor thermal alteration of magnetic minerals, low-field magnetic susceptibility was measured after each heating step using a Bartington Instruments MS2B meter. In addition, to confirm the magnetic composition deduced from the Lowrie method, some low-temperature (5–300 K) magnetic measurements were conducted on magnetic extracts using a Quantum Design SQUID VSM. Magnetic extracts were cooled from room temperature to 5 K in zero-field in the SQUID VSM. At 5 K, a 5 T DC field was applied and then switched off to impart a low-temperature saturation isothermal remanent magnetization (LT-SIRM). The LT-SIRM curves were measured during warming in zero field up to 300 K at a warming rate of 3 K/min to detect magnetic transition revealed from magnetic extracts.

All magnetic remanences of specimens including the composite magnetizations described above and the natural remanent magnetizations (NRM) were measured using a 2G Enterprises SRM-755 superconducting rock magnetometer. To evaluate the stability of NRM, thermal and alternative-field (AF) demagnetization methods were performed respectively on pilot samples from each site to provide information about which method is appropriate for the rest samples during paleomagnetic analysis. Over 10 demagnetizing steps from room temperature up to 600 °C (thermal demagnetization) or from 0 mT up to 100 mT (AF demagnetization), or first up to 290 °C and then up to 100 mT (thermal + AF demagnetization) were carried out and the remanent magnetizations after demagnetization were measured subsequently.

4. Results

4.1. Rock magnetic properties and magnetic mineralogy

The values of km and NRM of all specimens fall in the range of 49.1–671.7 10^{-6} SI and 0.05–8 mA/m, respectively. Except for a few sites in the Plio-Pleistocene Cholan and the latest Miocene Kueichulin formations that have relatively large values, most sites older than the Kueichulin formation have weak values (K_m: 255 10^{-6} SI; NRM: 0.3 mA/m), implying that these sites contain rather low concentrations

Table 1
Results of paleomagnetic analyses. Data from this study (Ref 1), Hsu et al., Lue et al., 1995 (Ref 2), Lee et al., 1991 (Ref 3), Hsu et al., 1966 (Ref 4), Miki et al., 1993 (Ref 5) and Horng, 2014 (Ref 6). Name: site label; S_0: dip direction and dip of the bedding. N/N_0: number of selected specimens for site mean calculation on the total number of measured specimens; when there are no direction information in the following columns the N value represents the number of specimens providing a representative component of magnetization. L_{com} and H_{com}: *in situ* declination and inclination of the L and H components respectively; α_{95}: angular confidence; κ: dispersion parameter; %: selected step of unfolding of the bedding for the record of the magnetization, L_{com} are recorded at 0% of bedding unfolding so before any bedding correction; rot: amount and sense of rotation calculated from the apparent polar wander path for East-Asia (Cogné et al., 2013); Δ_I: inclination of reference (calculated from the apparent polar wander path for East-Asia) minus the component inclination; Rot and Δ_I uncertainties have been corrected according Demarest (1983), the references at 10 and 20 Ma have been used for magnetizations recorded at 100% of unfolding and the references at 0 and 10 Ma have been used for others.

Site information		L-component magnetizations results						H-component magnetizations results						Ref
Name	S_0	N/N_0	L_{com}	α_{95}	κ	rot	Δ_I	N/N_0	H_{com}	α_{95}	κ	%	rot	Δ_I	
Wanli-Shangchi area (A area) – Fig. 11															
A1	170/13	4/10	360/28	13	54	−1 ± 6	15 ± 5	3/10	140/−38	18	51	0	−40 ± 11	4 ± 9	1
A2	160/25	5/9	353/29	7	111	−8 ± 6	14 ± 4	1/9							1
A3	130/15	1/10						9/10	0/43	7	63	100	11 ± 9	−12 ± 4	1
A4	145/22	9/10	353/25	11	23	−8 ± 6	18 ± 6	6/10	226/−38	12	31	100	42 ± 7	0 ± 6	1
A5	143/33	10/15	347/37	6	60	−14 ± 6	5 ± 4	10/15	201/−23	11	19	100	36 ± 7	2 ± 6	1
A6	154/21	19/20	10/27	5	46	9 ± 5	16 ± 3	18/20	210/−29	9	16	100	40 ± 6	1 ± 5	1
A7	313/24	3/21						18/21	202/−21	7	28	0	22 ± 5	21 ± 4	1
A8	328/56	17/17	351/26	5	49	−10 ± 5	16 ± 3	17/17	148/−27	7	25	0	−32 ± 5	16 ± 4	1
A9	159/35	9/10	5/38	15	13	4 ± 10	4 ± 8	9/10	205/−7	10	29	100	29 ± 6	13 ± 5	1
A10	350/54	7/10	190/−45	15	17	10 ± 14	−2 ± 9	2/10							1
A11	143/55	11/14	350/43	7	48	−11 ± 6	0 ± 4	14/14	188/−13	7	24	100	26 ± 6	2 ± 4	1
A12	149/36	5/10	141/−35	17	22	−39 ± 12	7 ± 10	7/10							1
A13	157/46	3/12						10/12	207/−18	13	21	100	43 ± 10	1 ± 8	1
A14	160/34	0/12						0/12							1
A15	93/8	12/12	343/28	6	52	−18 ± 5	14 ± 4	12/12	157/−23	9	26	0	−2 ± 6	16 ± 5	1
A16	325/22	2/15						10/15	33/30	9	34	0	32 ± 6	12±5	1
A17	4/58	16/18	10/32	7	30	9 ± 5	10 ± 4	13/18	292/−66	12	14	100	33 ± 9	4 ± 7	1
A18	122/43	7/17						9/17	177/−36	14	16	100	34 ± 12	−9 ± 8	1
A19	331/65	11/12	354/49	8	36	−7 ± 7	−7 ± 5	10/12	207/−39	14	16	0	18 ± 9	−3 ± 6	1
A20	336/42	1/10						0/10							1
A21	105/70	6/10						6/10							1
A22	131/41	12/16	2/38	10	22	2 ± 7	4 ± 6	10/16	131/−45	16	11	0	−50 ± 12	1 ± 9	1
A23	239/60	4/10	129/−28	14	57	−52 ± 10	15 ± 7	6/10	222/−41	19	18	0	42 ± 13	−2 ± 10	1
A24	160/40	10/14	358/47	9	32	−3 ± 8	−5 ± 7	1/14							1
Tl	150/20														2
Ts8607	148/50							7/	203/11	13	22	100	26 ± 7	10 ± 6	3
Ts8608	148/50							6/	220/14	12	32	100	37 ± 6	26 ± 6	3
Wc01	151/27							6/9	154/−34	8	78	0	−21 ± 6	4 ± 5	2
Wc02	151/27														2
Taoyuan area (B area) – Fig. 12															
B1	310/38	7/8	351/21	14	19	−10 ± 7	22 ± 6	8/8	136/−20	12	23	65	−36 ± 9	−4 ± 6	1
B2	138/23	1/12						10/12	147/−21	13	18	100	−33 ± 10	−3 ± 8	1
B3	125/54	2/7						5/7	160/−67	15	21	45	−43 ± 14	−4 ± 10	1
B4	306/78	10/14	336/44	16	1	−26 ± 11	−4 ± 8	11/14	249/−18	9	25	100	26 ± 6	5 ± 5	1
B5	151/35	12/13	353/41	6	61	−8 ± 5	2 ± 4	10/13	181/2	13	16	100	3 ± 6	11 ± 6	1
B6	344/72	16/18	345/33	5	6	−16 ± 5	9 ± 3	12/18	237/−41	12	24	5	19 ± 6	−6 ± 4	1
B7	290/31	10/11	346/28	8	43	−15 ± 6	14 ± 4	8/11	234/−42	18	10	100	20 ± 17	−11 ± 10	1
B8	292/46	11/13	356/37	4	147	−4 ± 4	5 ± 3	12/13	356/37	4	147	40	21 ± 5	−7 ± 3	1
B9	303/12	9/10	35/34	5	155	−1 ± 5	8 ± 3	7/8	207/−44	15	17	100	15 ± 10	2 ± 8	1
B10	136/54	17/17	173/−18	8	22	−7 ± 5	24 ± 4	16/17	328/−10	9	20	80	−34 ± 5	17 ± 4	1
B11	262/58	17/17	167/−17	9	19	−14 ± 6	25 ± 5	11/17	221/20	10	24	100	36 ± 6	13 ± 5	1
B11-H2	262/58							10/17	325/21	7	53	0	−35 ± 5	21 ± 4	1
Nt23	177/12							7/	167/−24	4	203	90	−6 ± 3	3 ± 3	5
Nt24	137/24							9/	19/−43	4	185	0	10 ± 5	2 ± 3	5
Nt25								7/	2/12	6	113	100	−11 ± 3	−1 ± 3	5
Nt47	319/59							4/	271/−53	11	73	100	−1 ± 9	−10 ± 6	5
St01	140/40							8/	325/6	6	76	90	−31 ± 6	−2 ± 4	2
St02	140/40							8/	333/1	4	258	90	−22 ± 4	−3 ± 3	2
St03	146/69														2
St04	146/69							7/	153/18	7	70	90	−26 ± 6	−4 ± 4	2
St05	220/37							10/	166/10	3	353	90	−26 ± 3	11 ± 2	2
St06	220/37							8/	165/9	2	705	90	−25 ± 2	13 ± 2	2
St07	220/37							5/	186/−24	12	45	90	−14 ± 10	−10 ± 6	2
St08	220/37							8/	195/−22	5	149	90	−1 ± 5	−12 ± 3	2
St10	220/37							6/	179/−14	11	39	90	−16 ± 7	1 ± 6	2
St11	144/74							7/	155/16	6	95	90	−21 ± 6	−9 ± 4	2
St18	156/80														2
St19	180/47							7/	165/4	6	100	90	−18 ± 5	7 ± 4	2
St20	166/56														2
Ts8611															3
Ts8612															3
Hsinchu area (C area) – Fig. 13															

(continued on next page)

Table 1 *(continued)*

Site information		L-component magnetizations results						H-component magnetizations results						Ref
Name	S_0	N/N_0	L_{com}	α_{95}	κ	rot	Δ_I	N/N_0	H_{com}	α_{95}	κ	%	rot	Δ_I	
C1	136/73	4/17						13/17	323/42	12	30	0	−38 ± 9	−2 ± 6	1
C2	355/22	2/17						17/17	153/−28	1	13	0	−28 ± 6	13 ± 6	1
C3	318/23	16/26	6/44	6	35	5 ± 6	−1 ± 4	16/26	228/−52	6	38	100	18 ± 6	−8 ± 4	1
C4	150/72	14/17	165/−27	8	28	−13 ± 8	17 ± 6	16/17	27/1	8	24	100	47 ± 5	7 ± 4	1
C5	145/85	3/16						2/16							1
C6	305/84	0/17						6/17	254/−23	24	10	45	51 ± 17	−2 ± 12	1
C7	314/79	1/17						14/17	77/−5	8	28	100	53 ± 5	6 ± 4	1
Chiaopanshan area (Ch area) – Fig. 16															
Ch3	300/34							4/	203/10	7	89	100	22 ± 5	40 ± 4	4
Ch4	267/32							6/	227/−12	5	128	100	37 ± 5	7 ± 3	4
Ch5	265/31							4/	216/−34	12	34	70	18 ± 10	−4 ± 6	4
Ch6	300/30							6/	216/−49	2	943	55	18 ± 4	−4 ± 3	4
Ch7	270/27							5/	196/−3	6	129	100	1 ± 5	22 ± 3	4
Ch8	161/42							4/	168/26	6	130	100	−12 ± 5	26 ± 4	4
Ch9	161/42							6/	169/47	6	100	100	−16 ± 5	13 ± 4	4
Ch10	161/42							7/	170/0	5	130	100	−8 ± 5	2 ± 3	4
Ch11	160/40							4/	140/−15	8	70	65	−45 ± 7	−2 ± 5	4
Ch12	160/40							3/	149/−27	7	122	35	−33 ± 6	−2 ± 5	4
Ch13	160/40							9/	178/12	8	35	100	−3 ± 5	22 ± 4	4
Ch14	160/40							3/	146/8	13	41	100	−36 ± 7	12 ± 6	4
Nt01	161/49							7/8	196/6	3	378	100	21 ± 3	5 ± 2	2
Nt02	161/40														2
Nt03	161/42							8/8	148/0	3	301	100	1 ± 4	−10 ± 2	2
Nt04	161/42							9/9	163/7	3	316	100	−20 ± 3	−4 ± 2	2
Nt05	161/42							8/8	149/−23	6	97	35	−46 ± 7	−5 ± 4	2
Nt06	161/42							8/11	17/1	12	24	100	13 ± 6	24 ± 5	2
Nt07	205/28							9/9	194/2	5	117	100	10 ± 3	19 ± 3	2
Nt08	220/22							8/9	176/−17	9	40	100	−15 ± 6	18 ± 5	2
Nt09	220/22							3/5	179/−37	13	90	100	−25 ± 1	−1 ± 6	2
Nt10	168/46							10/10	244/−44	5	89	0	63 ± 6	−3 ± 4	2
Nt12	326/80							7/7	273/−26	13	24	100	28 ± 8	2 ± 6	2
Nt13	319/30														2
Nt14	155/30														2
Nt15	168/46														2
Nt43	160/34							7/	165/−26	3	543	0	−16 ± 4	16 ± 3	5
Nt44	160/34							7/	174/−9	3	323	100	−2 ± 4	2 ± 3	5
Nt46	205/28							10/	197/11	6	61	100	16 ± 5	26 ± 16	5
Ty03	146/68							6/13	164/13	7	84	100	−16 ± 5	14 ± 4	2
Ty04	131/22							11/12	39/21	7	39	100	35 ± 6	−2 ± 4	2
Ty05	136/68							8/8	143/35	10	32	100	−40 ± 6	6 ± 5	2
Miaoli area (D area) – Fig. 14															
D1	100/34	4/16	345/2	13	49	−15 ± 6	40 ± 6	10/13	170/−22	12	21	100	6 ± 11	12 ± 10	1
D2	125/65	2/8						5/8	358/16	13	35	100	33 ± 9	0 ± 6	1
D3	126/65	3/10													1
D4	111/87	17/27	2/39	7	31	1 ± 6	3 ± 4	12/27	222/−16	9	24	50	41 ± 6	26 ± 5	1
D5	115/51	2/13						11/13	182/−18	9	26	100	24 ± 5	11 ± 5	1
D6	275/24	7/17	4/34	13	23	3 ± 8	7 ± 6	6/17	223/−26	18	15	100	28 ± 11	1 ± 9	1
D7	133/19	16/21	359/25	22	8	−2 ± 6	16 ± 5								1
D8	110/27	7/17	273/−34	11	53	94 ± 14	10 ± 7	15/17	196/−24	6	37	100	26 ± 4	17 ± 3	1
D9	125/75	12/22	349/43	8	29	−12 ± 9	2 ± 6	18/22	179/−36	10	14	50	32 ± 9	−8 ± 6	1
D10	35/36	14/16	359/38	6	49	−1 ± 5	4 ± 4	15/16	150/−60	11	14	100	−3 ± 6	1 ± 6	1
Taichung and Nantou area (E and F area) – Fig. 15															
E1	140/48	3/16						11/16	352/31	8	31	20	−5 ± 6	3 ± 5	1
E2	184/22	1/16						16/16	182/−15	8	24	100	1 ± 6	4 ± 5	1
E3	235/35	0/16						15/16	155/−41	8	24	0	−25 ± 6	2 ± 5	1
F2	108/30	1/15						3/15							1
F3	295/9	2/11						9/11	189/−51	10	25	100	−4 ± 8	−10 ± 6	1
F4	300/55	0/11						4/11							1
F5	262/78	1/8						1/8							1
Fei-Tsui reservoir area (Ft area) – Fig. 17															
Mc01	165/40							8/8	178/3	5	105	100	−2 ± 4	3 ± 3	2
Mc03	180/32							9/11	219/1	10	30	100	41 ± 5	16 ± 5	2
Mc04	180/32														2
Ti01	215/41														2
Ti02	0/23							7/8	143/−62	6	116	100	−27 ± 5	−5 ± 3	2
Ti03	346/30														2
Ti04	37/32														2
Ti05	134/30														2
Ti06	123/24							8/10	179/−49	9	43	100	26 ± 10	−16 ± 6	2

(continued on next page)

Table 1 *(continued)*

Site information		L-component magnetizations results						H-component magnetizations results							Ref
Name	S_0	N/N_0	L_{com}	α_{95}	κ	rot	Δ_I	N/N_0	H_{com}	α_{95}	κ	%	rot	Δ_I	
Ti07	112/30														2
Ti08	170/50							8/10	189/−6	5	118	100	17 ± 5	−14 ± 3	2
Ts8609	350/34							4/	260/−75	18	26	100	14 ± 17	−14 ± 10	3
Ts8610	118/25														3
Keelung volcano group area (Ke area) – Fig. 3															
Bsn								2/	22/34	6	268	100	22 ± 5	9 ± 4	4
Bsr								4/	198/−19	21	11	100	18 ± 10	23 ± 10	4
BU								12/	203/−23	8	29	100	22 ± 5	19 ± 4	4
Kln								5/	/59	13	25	100	- ± 15	17 ± 1	4
Kp01								8/8	23/24	10	30	0	22 ± 6	19 ± 5	2
Kp02								6/8	30/11	12	32	0	29 ± 6	31 ± 6	2
Kp03															2
Kp04															2
Kp05															2
Kp06															2
Nt40		9/	3/53	6	110	2 ± 6	−11 ± 4								5
Tsr								3/	203/0	10	66	100	23 ± 6	42 ± 5	4
Wt								6/	179/−44	17	11	100	−2 ± 13	−2 ± 9	4
Tali coast area (Ta area)															
KPS07	320/10							7/8	19/45	6	97	100	18 ± 6	−3 ± 4	2
TS8601	148/50							5/	217/−12	21	14	0	28 ± 10	23 ± 10	3
TS8604	330/23							3/	192/−20	28	19,9	0	1 ± 24	7 ± 15	3
TS8722	344/26							5/	194/−22	2	15	0	6 ± 15	3 ± 10	3
TS8725	17/14							4/	187/−25	23	1	0	1 ± 14	9 ± 11	3
Tatun-Linkou area area (T-L area) – Fig. 2															
Ahp								6/	8/29	9	40	0	8 ± 6	14 ± 5	4
Ahy								2/	356/44	6	268	0	−5 ± 6	−2 ± 4	4
Ap								4/	356/47	7	96	0	−5 ± 6	−4 ± 5	4
Aph								2/	337/33	14	54	0	−24 ± 1	10 ± 6	4
Apho								2/	4/6	2	3617	0	3 ± 4	37 ± 2	4
Aphs								9/	3/34	9	27	0	3 ± 6	9 ± 5	4
B1								7/	13/53	3	271	0	12 ± 5	−10 ± 3	4
B2								12/	6/51	4	137	0	5 ± 5	−8 ± 3	4
B4								8/	359/45	2	701	0	−2 ± 4	−3 ± 3	4
B5								8/	6/50	2	754	0	5 ± 4	−8 ± 2	4
B7								2/	29/24	1	771	0	29 ± 4	−19 ± 2	4
Ba								6/	5/41	10	36	0	4 ± 7	2 ± 6	4
KYS06	130/30							6/8	331/63	2	864	0	−28 ± 6	19 ± 4	2
Tananwan								12/19	186/−39	5	62	0	6 ± 5	4 ± 4	6

of ferrimagnetic minerals. These results are consistent with the observations of Lee et al. (1991) and Lue et al. (1995) for the same rock formations.

The low magnetic concentrations for those older sites also result in quite noisy hysteresis loops, which are close to the detect limit of the vibrating sample magnetometer for 0.4–2.4 g bulk specimens. Magnetic extracts separated from different rock formations, however, enhance the signals and exhibit very narrow steep loops that are almost fully saturated before 0.5 T after high-field slope correction (Fig. 5). The Day plot using the ratios of hysteresis parameters (M_{rs}/M_r vs. H_{cr}/H_c) further reveals that magnetic grain sizes are mainly in the range of pseudo-single domain but some extend to the range of mixing of single domain and superparamagnetic state (Day et al., 1977; Dunlop, 2002).

Thermal demagnetization of the composite IRM indicates that the

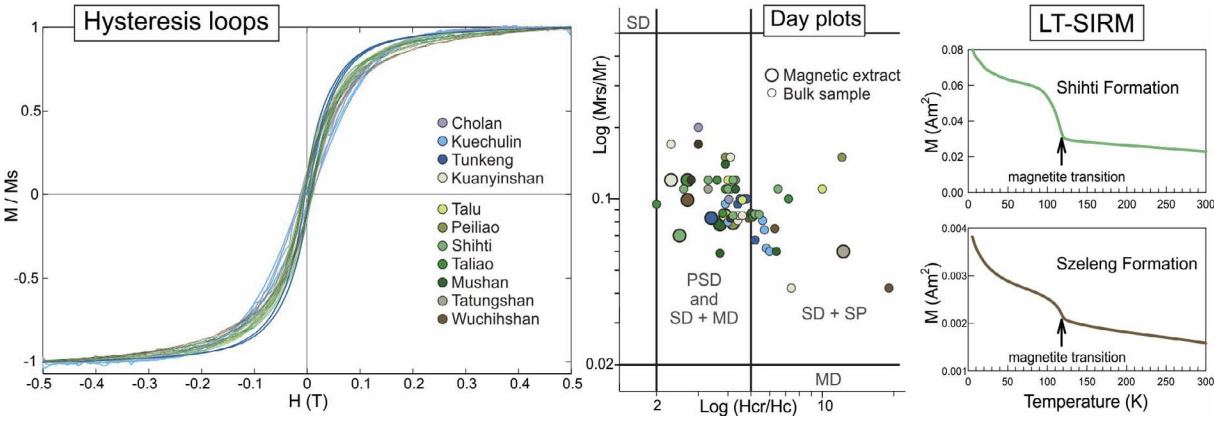

Fig. 5. Rock magnetism properties. Weighted hysteresis loops after dia/paramagnetic adjustement, Day plots (M_{rs}/M_r–H_{cr}/H_c diagrams) and low-temperature analysis of SIRM.

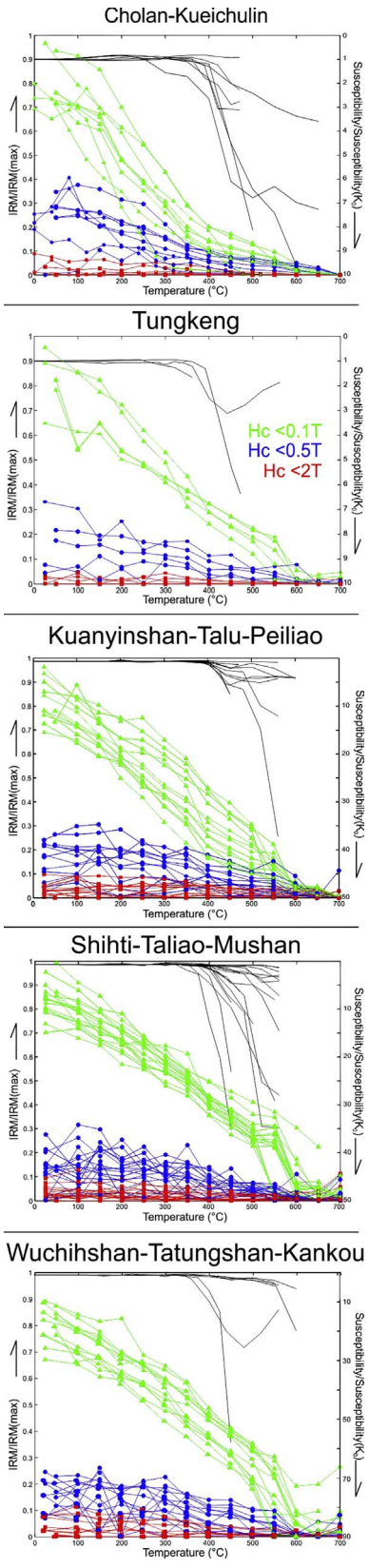

Fig. 6. 3 axis thermal demagnetization curves (Lowrie's method, 1990) and magnetic susceptibility evolution during thermal demagnetization. All the results are presented after normalization of the respective highest value.

soft (H_{cr} < 0.1 T), medium (0.1 T< H_{cr} < 0.5 T) and hard (0.5 T< H_{cr} < 2 T) coercivity components contribute about 70–90%, 10–30%, and 0–10% respectively to the total signal for all of studied formations (Fig. 6). Most of thermal demagnetization patterns show that the soft and medium coercivity components first decrease steadily from the room temperature to 550 °C, and then decrease abruptly between 550 °C and 600 °C. Such magnetic behaviors are interpreted that magnetic mineral is predominated by low-coercivity magnetite with a wide range of unblocking temperatures. However some patterns as shown in the Cholan-Kueichulin formations (Fig. 6) decrease significantly before 400 °C, which could be resulted from thermal decomposition of low unblocking temperature magnetic minerals like titanomagnetite. Thermal alteration during heating is also common for all sites as shown by the significant increase of magnetic susceptibility higher than 350–400 °C (Fig. 6), indicating that new magnetic minerals could form due to the heating alteration of non-magnetic phases like siderite or pyrite (Pan et al., 2000). However, these newly formed magnetic minerals apparently do not affect the demagnetization behaviors of the IRMs before 600 °C. The LT-SIRM curves through low-temperature magnetic measurements on magnetic extracts clearly show the Verwey transition at 115 K (Verwey, 1939, Fig. 5). These results confirm that magnetite is the dominant magnetic carrier in the different stratigraphic formations of the NTFS.

4.2. Characteristics of remanent magnetizations

Based on the preliminary results of the pilot specimens, we have treated 7–27 specimens per site with either AF or thermal or a mix of AF and thermal demagnetization to obtain the site mean remanent direction. Although a total of 21% specimens have been discarded due to unstable magnetizations, the rest of specimens display stable remanent components. However in some case, the signal remains a bit chaotic to allow different possible interpretation, like F4-3a or D8-14b in Fig. 7. Representative or characteristic remanence for each specimen was determined using the Paleomac software (Cogné, 2003) that includes the principal component analysis and the great circle fitting (Halls, 1978; Kirschvink, 1980). As shown in Fig. 7, two main types of demagnetization behaviours can be usually observed on the specimens. Type I has a listric-shape decreasing magnetization and type II first has an increase of the magnetization and then a decrease during the demagnetization processes. Regardless of the types, two different components of magnetization, named as L- and H-components which are highlighted with red and blue segments respectively in Fig. 7, can be identified for most of specimens. Fisher statistics, great circle intersection of vectors, or mixed average of vectors and great circles were then used to calculate the average direction of the L- and H-components for each site (Fisher, 1953; McFadden and McElhinny, 1988). The paleomagnetic results for all of sites in the NTFS including this study and others (Hsu et al., 1966, 1991, 1993, 1995, 2014, i.e.) are summarized in Table 1.

For the L-component, it is characterized by a low coercivity or a low unblocking temperature (2–30 mT or 25–240 °C; Fig. 8), implying it was acquired through a late re-magnetization of specimens. In general, the sites bearing with this component have a smaller statistic uncertainty and 61% of the sites have the $\alpha_{95} \leq 10°$. The stereographic projection of the L-components before and after bedding correction further confirms that this magnetization was acquired after folding/tilting of the bedding and most of L-components have a normal magnetic polarity, with exceptions for the sites A10, A12, A23, B10, B11, C4 and D8 (Fig. 8). Detailed interpretations for these sites will be discussed in the following sections. By contrast, the H-component has a higher coercivity or a higher unblocking temperature, and therefore can be regarded as the characteristic remanent magnetization of the specimens. When previous studied sites (Hsu et al., 1966; Lee et al., 1991; Miki et al., 1993; Lue et al., 1995; Horng, 2014, see Table 1) were taken into account, the H-components display either a reversed or a normal magnetic polarity in situ. H-components have a slightly larger statistic uncertainty of alpha95 (i.e. 47% of sites have $\alpha_{95} \leq 10°$).

Actually the quality of the H-components remains questionable especially at the site scale with a low dispersion parameter, in general

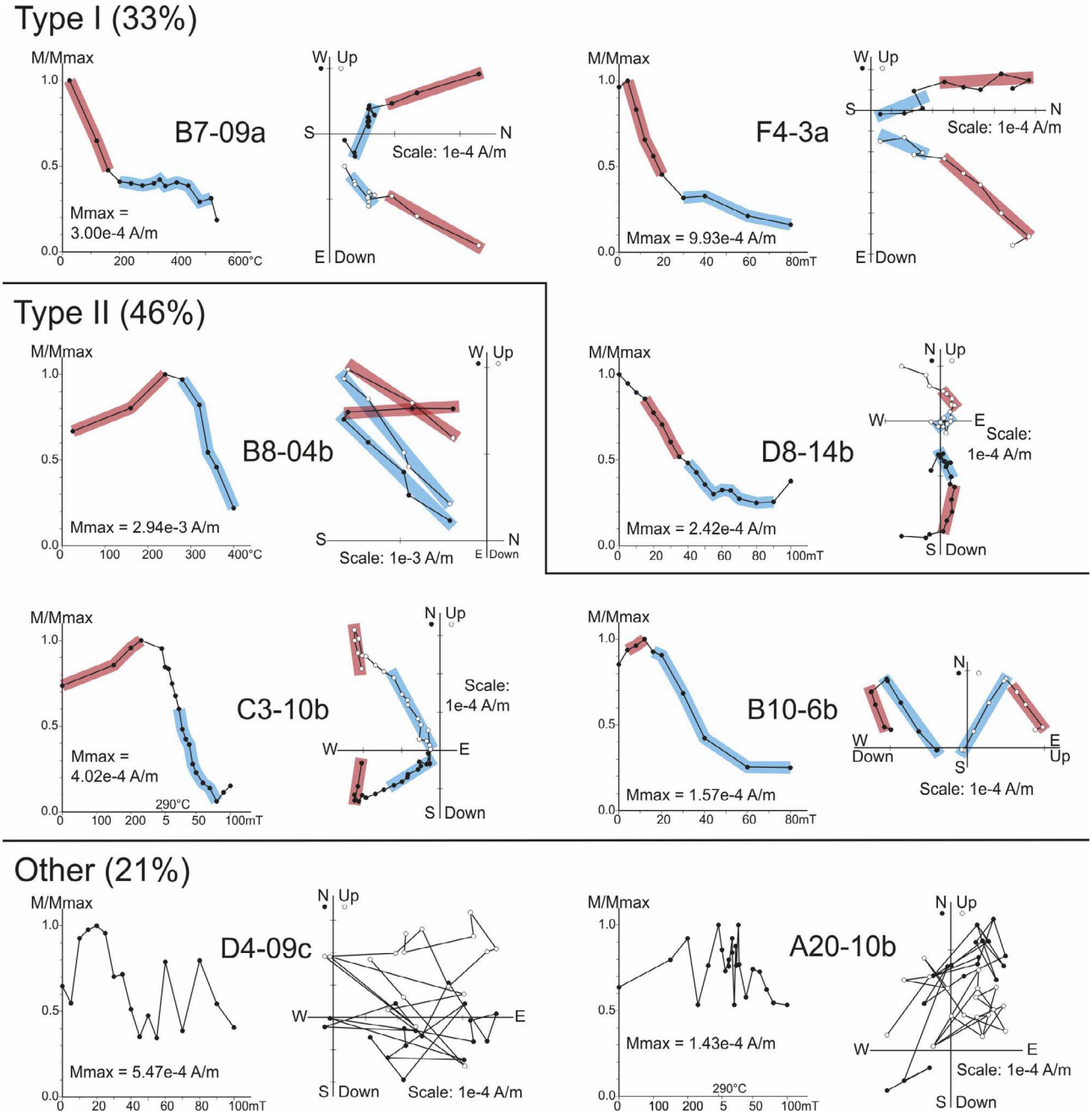

Fig. 7. Examples of the most representative demagnetization profiles and Zijderveld plots. Percentages correspond to the occurrence of the different demagnetization profiles. Red highlight correspond to L-component and blue highlight correspond to H-component.

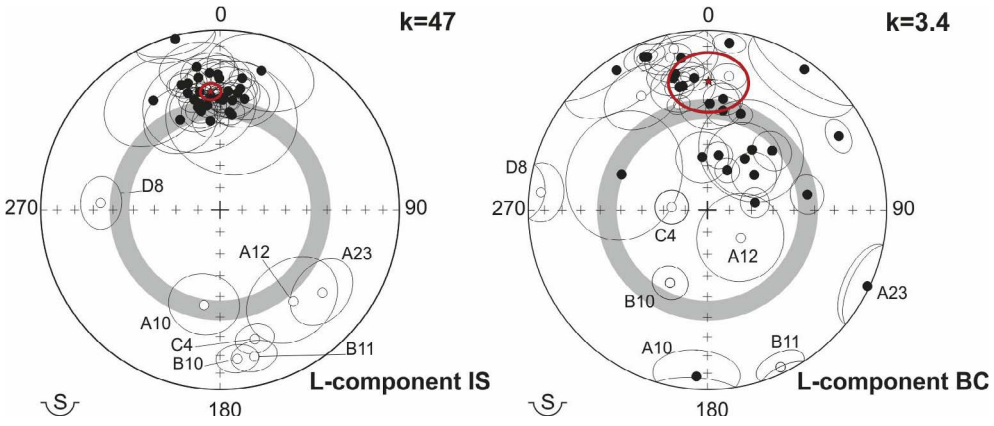

Fig. 8. Stereographic projections of the L-components *in situ*, IS, and after bedding correction, BC. The expected magnetization, inclination and declination, for 0 and 10 Ma are represented by the grey circle.

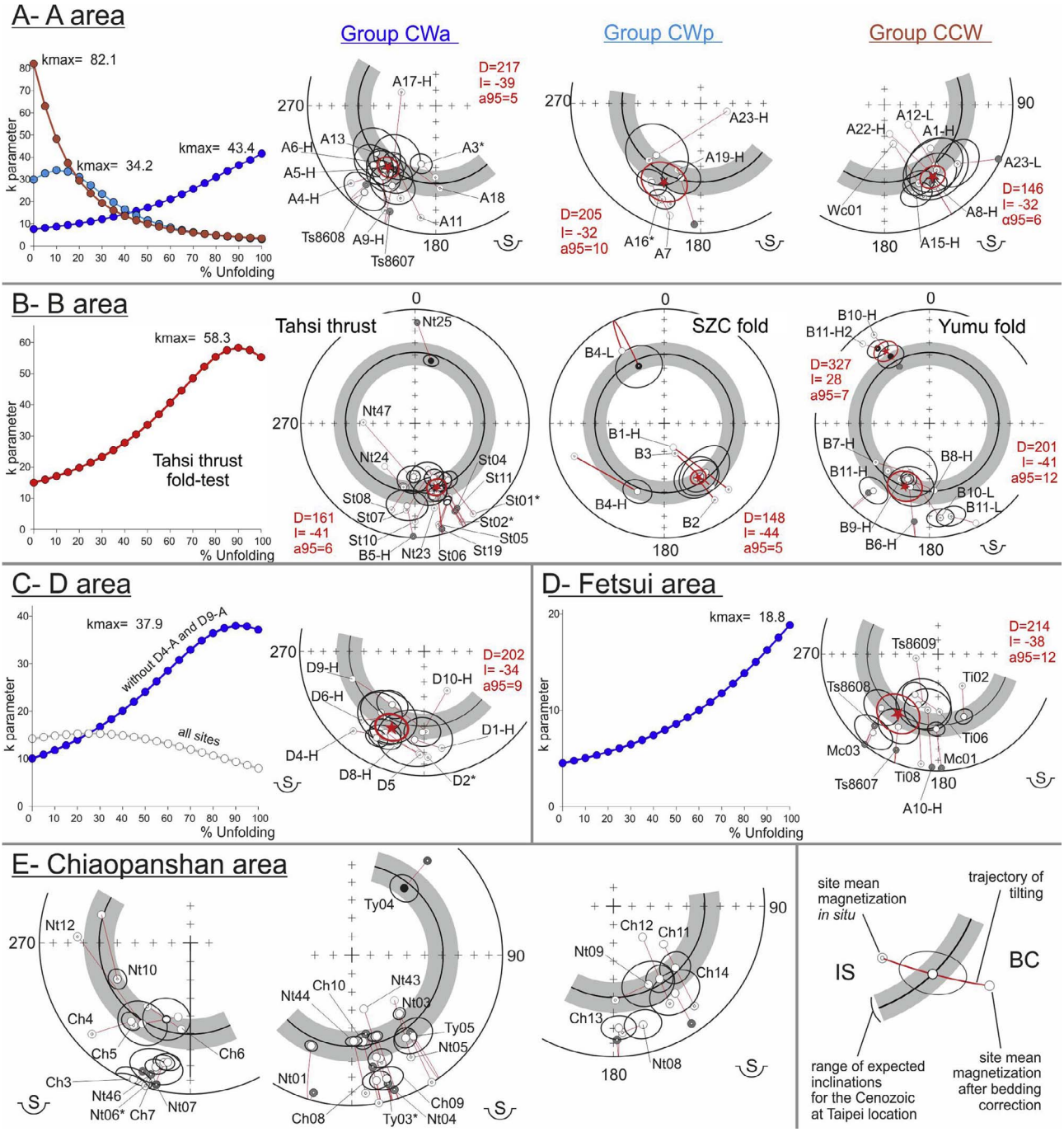

Fig. 9. Fold test for the different studied areas. The diagrams show the results of the fold test with the evolution of the dispersion parameter, κ, for a progressive symmetrical unfolding and the tilting trajectories of the components of magnetization of the corresponding sites in stereographic projections. In the stereographic projection both the components of magnetization *in situ*, IS, after bedding correction, BC, and the selected configuration are presented. The selected configuration for final average calculation are drew in black whereas other configurations are drew in grey. The uncertainties are only shown for the selected configuration. The symbol * indicates that the data has been rotated by 180°. The expected inclination for 0–40 Ma are represented by the grey circle.

between 20 and 60, and sometimes even between 10 and 20. According to the recommendations proposed by Pueyo et al. (2016), such low values allow doubt on their reliability. A quick comparison with the previous studies (Table 1) highlights the presence of better dispersion parameter exceeding 100. The reasons are (1) that most of them sampled exclusively magnetic formation with a stronger signal as volcanic formation, and (2) they were more selective on the number of selected specimens generally less than 10 and often under 6. Although our dispersion parameter are low, we consider as much specimen as possible rather to artificially improve the statistic parameters with an excessive selection. We attribute the poor quality of the magnetic signal to the weakness of remanent magnetization intensities, the high concentration of soft and low blocking temperature magnetic contributions, and the presence of super-paramagnetic grains.

4.3. Fold-test and block horizontal rotation

A fold/tilt test associated with bedding correction (McFadden and Jones, 1981) has been carried out (Fig. 9). The resulting tilting/folding trajectories in the stereo-plots have been used to decipher the record of

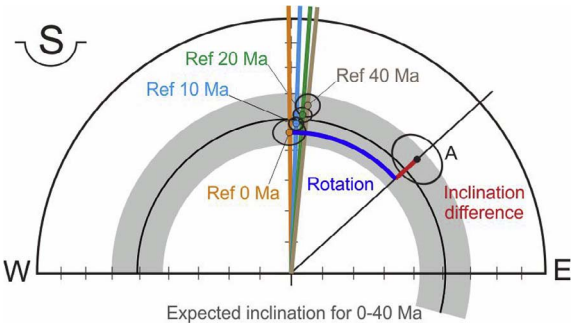

Fig. 10. Magnetization of reference for SE Asia at North Taiwan location. Temporal evolution of the paleomagnetic directions from Eocene to present at the latitude of Taipei, calculated from the apparent polar wander path for East Asia (Cogné et al., 2013). The grey circle corresponds to the expected range of inclination for Cenozoic time used for deciphering the consistency of our paleomagnetic results. The rotations are calculated as the difference in azimuth between a magnetization, A in this example, and one of the characteristic direction from Eocene to present. The inclination difference corresponds to the angle between the inclination of A and the selected characteristic direction. The symbol S in an hemispheric shape indicates that a Schmidt or equal area stereographic inferior projection has been used.

the magnetizations. In addition to our samples, we also made a re-determination for the samples analyzed by previous authors (T-L, Ft and Ch areas in Fig. 1) improved by the consideration of the tilting trajectory of the magnetizations. For the Tatun-Linkou (T-L), Feitsui reservoir (Ft) and Chiaopanshan (Ch) areas, the bedding planes of the corresponding sites have been either collected from the different publications when provided or determined from the local 1:50,000 geological maps. The declination and inclination values of remanence of each site were compared with the reference geomagnetic field (i.e., virtual geomagnetic pole) for East Asia at the latitude of Taipei (Cogné et al., 2013, Fig. 10) to determine the amount of horizontal block rotation. The uncertainties of rotation were estimated according to the correction proposed by Demarest (1983).

4.3.1. Wanli-Shangchi area (A-area)

The A-area is the most intriguing and representative studied area. It is also the area we sampled the most. The youngest sampled formation is the upper Miocene Nanchuang formation (also referenced as the Shangfuchi and Tungkeng formations in Central western Taiwan in Fig. 4, site A15), 6.5–11.4 Ma in age. Fold-tests have been performed on H-components and L-components of magnetization at sites A12 and A23 (Fig. 9-A). Initially, two main groups have been identified: (a) group CW (blue fans in Fig. 9-A), magnetic components with clockwise trend, declinations into the SE quadrant, and (b) group CCW (red fans in Fig. 9-A), components with counterclockwise trend, and declination into the SW quadrant. The fold test for group CCW (Fig. 9-A) shows unambiguously a magnetization record after folding. As a consequence, Group CCW is an overprint. The resulting average magnetization shows an inclination lower than the expected inclination for the 10–0 Ma period. The fold test for group CW (with clockwise trends) initially did not provide convincing result because this group includes H-component recorded either during latest stage of folding/tilting (Fig. 9-A, Group CWp) or before the folding (Fig. 9-A, Group CWa), both consistent in inclination with the expected magnetization for SE Asia. Group CWp is an overprint too.

Whatever the group no spatial or structural correlation can be obviously proposed, although two folds, Pinxi and Wanli folds, have been sampled. Nevertheless, the group CCW is rather located in the hinterland than Group CW, and syn- and post-folding magnetizations are often close to fold hinges or fault traces. One can also note that the declination of group CWa (217 ± 5°) is not significantly different to the declination of group CWp (205 ± 10°).

4.3.2. Taoyuan area (B-area)

West of the Taipei basin, the B-area includes both data we have collected and previous results from Lue et al. (1995). We distinguished three groups from the foreland to the hinterland according to the regional structural thrust sheets.

1. Shantzuchao fold. The group in foreland includes four sites, two in each limb of the Shantzuchiao fold (B1, B2, B3, and B4 at SZC fold in Fig. 12). The reverse H-components of magnetization indicate a syn-folding record of the magnetization at 65, 100 and 45% of back-tilting for the sites B1, B2 and B3, respectively (SZC fold in Fig. 9-B). These magnetizations are thus overprints. The B4-L component with normal polarity is interesting and reveals a good match with the mean of the B1-H, B2-H and B3-H components at ± 180° in declination (because of opposite polarity). The implications are that the record of the A-components magnetization occurred during a reversal coeval with the folding, then the record of the B4-L component magnetization occurred during a normal polarity period when the north limb was fully folded before the occurrence of a 20–30° counterclockwise horizontal rotation.
2. Tahsi thrust sheet. The group in the hanging wall of the Tahsi thrust is composed exclusively of the sites (St + Nt group) from the study of (Lue et al., 1995). The youngest formation they sampled is the Kueichulin formation (Fig. 4, St1-2-3-7-10-11-12-19-20 and Nt23-24), 3.5 to 6.5 Ma in age. As the authors had not performed the fold test, we conduct it using their data (Fig. 9-B). The results of our fold test indicate a counterclockwise rotation carried by ante-folding magnetization, or recorded during initial stage of folding/tilting. The resulting magnetizations are consistent in inclination and suggest a record of an average 21 ± 5° counterclockwise rotation, except for the sites Nt25 and Nt23 with no significant rotation (about + 5 ± 10°).
3. Yumu fold. Farther towards the hinterland across the Yumu fold (or Yumu syncline), two components of magnetization have been obtained (Table 1). The site B11 reveals an unusual magnetic pattern with 3 different components of magnetization (Fig. 12), and deserves particular attention. The first component is demagnetized before 200–240 °C. It is reverse polarity (*in situ*) and we attribute it to be B-comp. The second one is demagnetized before 470–520 °C. It is normal polarity (*in situ*) and is attributed to A2-comp. The third one is demagnetized over 550°C, it is poorly constrained by only 2–3 steps but it converges to the origin. It is reverse polarity after bedding back-tilt and thus we interpret it as H-comp. The H-comp indicates a clockwise rotation whereas the H2-comp and L-comp support the record of counterclockwise rotation. All of them present lower inclination by 5–20 °C with the expected inclination for SE Asia for the last 40 Ma.

For the fold test, most of the H-components of magnetization in the Yumu fold area did not provide a straightforward result, probably because the sites belong to different tectonic units. However, the analysis of the folding trajectories in stereographic plot (Yumu fold in Fig. 9-B) reveals that the paths of H-components at sites B6 and B8 cross each other at different unfolding stage, while the H-components at sites B7 and B9 are recorded before folding/tilting of the bedding. The flip of polarity of B11-H during back-tilting correction strongly supports a record of magnetization before folding/tilting. The resulting H-components of B11 indicate a record of a 23 ± 9° clockwise rotation.

The B11-H2 and some L-components (B10-L and B11-L) reveal better grouping before bedding back-tilt correction. On the other hand, B10-H suggests magnetization occurred during folding/tilting (80% of unfolding). They propose a record of a counterclockwise rotation of 30° ended before or during a magnetic pole inversion from normal (B11-H2 and B10-H) to reverse (B10-L and B11-L).

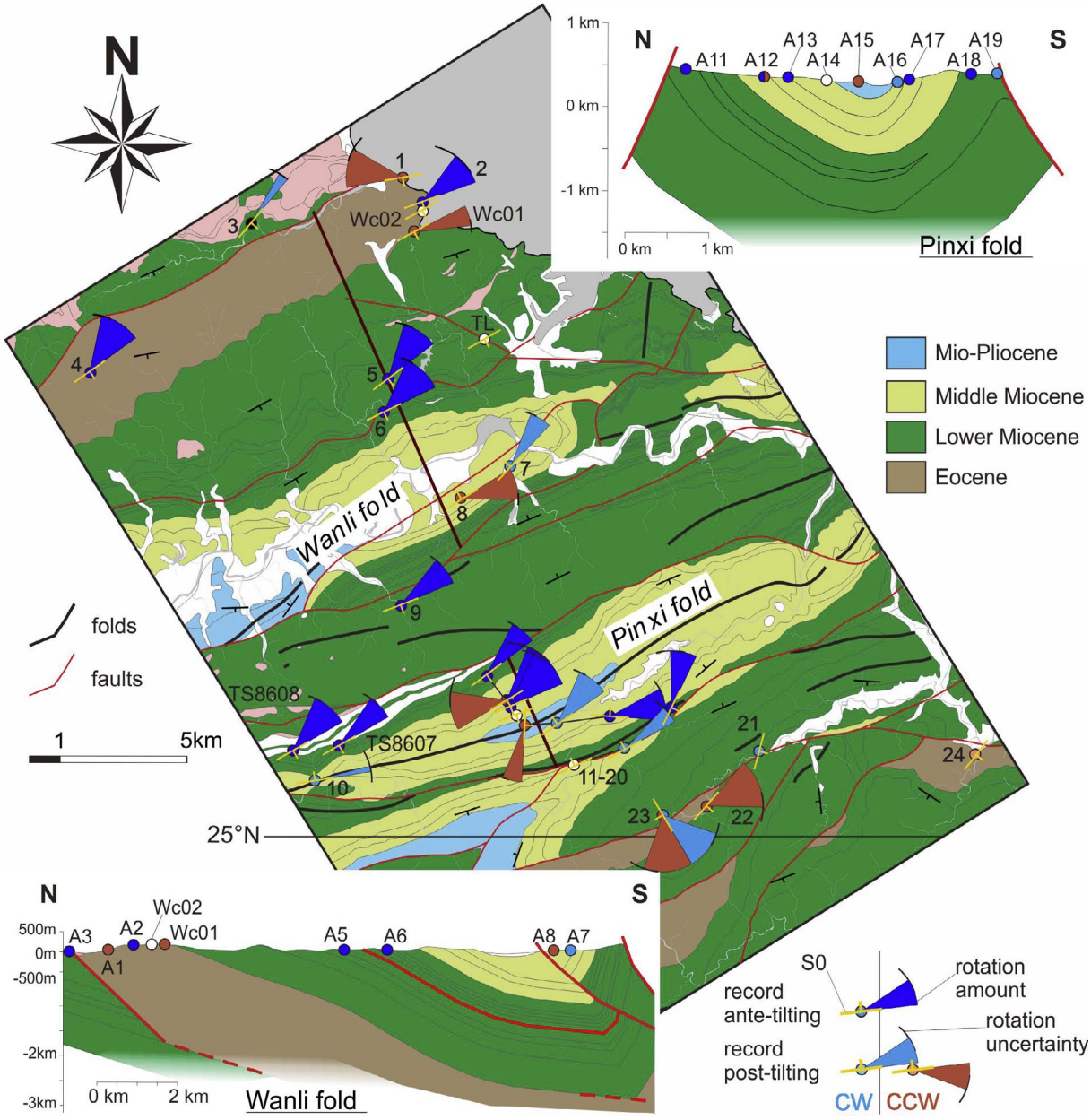

Fig. 11. Results of the analysis of the remanent magnetization for the A-area. Location, amount, sense and timing toward the folding of rotations are represented in the map and the corresponding cross-sections.

4.3.3. Hsinchu area (C-area)

Further south, we sampled along another cross-section in the C-area (Fig. 13). The youngest sampled formation is the Kuanyinshan formation (Fig. 4, sites C2–3), 11.4–13.9 Ma in age. The samples in this area provided the data with more complex signals to analyze, with least squares fitting in Zijderveld plot not sufficiently satisfied. As a result, the samples have been treated by great circle fitting for characterizing the components of magnetization and a mixed average of vectors and great circles intersections for calculating the average magnetization per site. In the first view the signals show very scattered behavior with components both in the west quadrant (C1, C3 and C6) and in the east quadrant, with both normal polarity (C1, C4-A and C7) and reversed polarity (C2, C3, C4-L and C6). The components C4-L and C2 show a clear prior to folding/tilting grouping whereas C4-H and C7 are obviously recorded after folding. The tilting paths of C6 and C3 in stereographic plot allow to add these components to the group of post-folding. Only one component, C5-H, could not be associated with any of these two groups. The path of bedding back tilting of the C5-H component suggests a record before folding/tilting but far from the other component and very low in inclination (about 20°); so this site was excluded for further calculations. The group of post-folding magnetization (C4-L, C1 and C2) are overprints and carries a 25 ± 11° counterclockwise rotation, lower by 11° with the expected inclination for 0–10 Ma. The C3, C4-H, C6 and C7 magnetizations are recorded at different tilting/folding stage and present a 50 ± 8° clockwise rotation, consistent in inclination with the expected values for SE Asia.

4.3.4. Miaoli area (D-area)

Further south, we sampled 10 sites in the D-area, including 1 site, D1, in the Cholan formation (1.1–2.6 Ma) and 4 sites, D2-3-4-6, in the Kueichulin formation (3.5–6.5 Ma, Fig. 4). The H-components are mainly reverse polarities, except D4-H after bedding back-tilt correction (Fig. 14). The fold test did not yield satisfied results (Fig. 9-C) due to the polarity of D4-H and the long tilting path of D9-H which evolves from

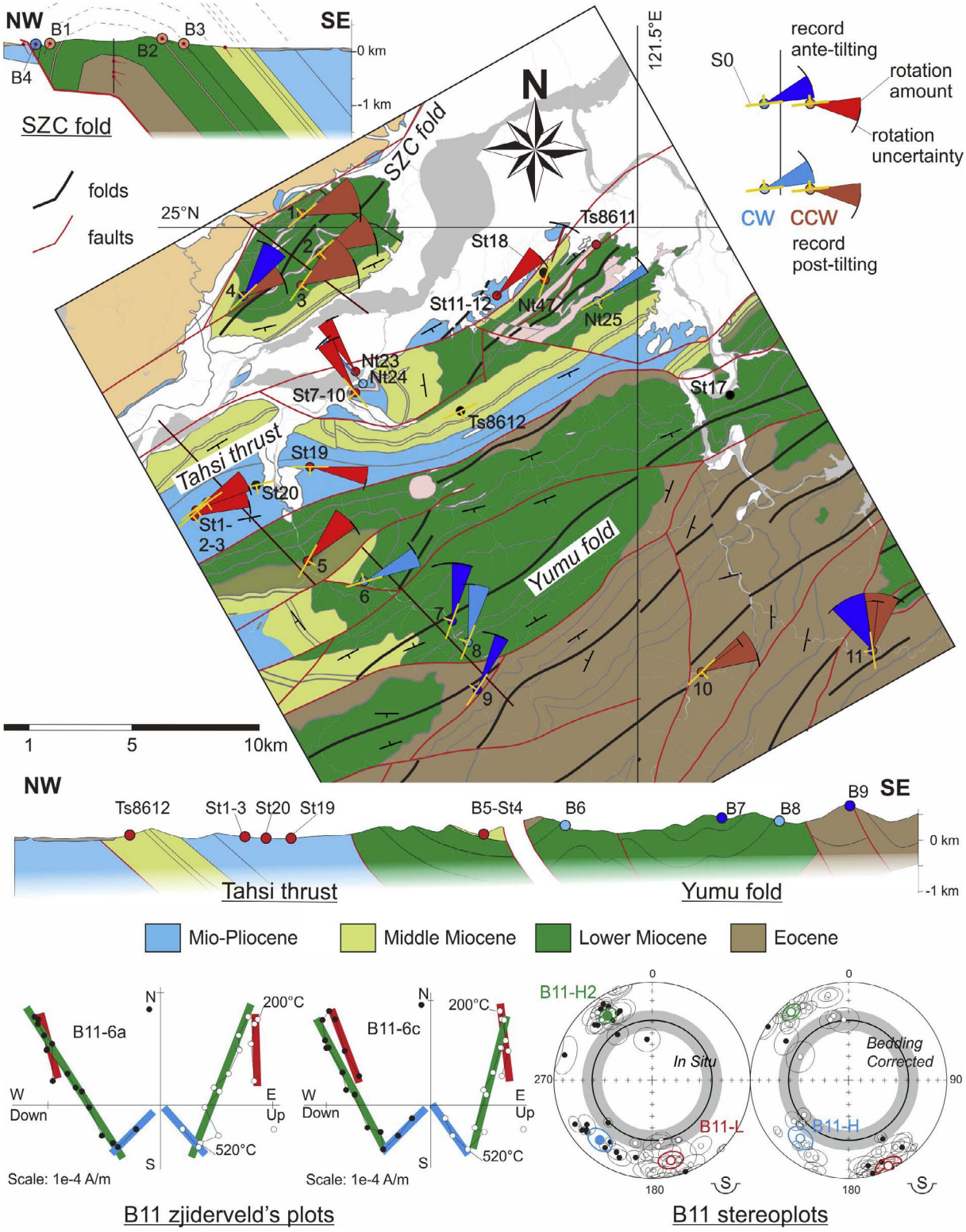

Fig. 12. Results of the analysis of the remanent magnetization for the B-area. Same legend as Fig. 11.

south-trending declination to WSW-trending declination, both consistent, in inclination, with the expected values for 0–20 Ma. The magnetization D4-H was recorded prior to titling/folding unless we consider a large horizontal rotation of more than 150°, which seems unlikely. For the magnetization D9-H, on the basis of the inclination consistency, either we consider a record before tilting with an important clockwise rotation or a record after tilting with no rotation. The fold test for the other sites reveals a better grouping after conducting bedding back-tilting correction, thus favors a record before folding or at least in the beginning of tilting of the strata. We can notice that, although the *in situ* inclination of D4-H is very low, its declination is consistent with those of the other sites. The same observation can also be made for D9-H, its position at 50% of the back-tilting path is very close to the grouping of the other sites. The corresponding average clockwise rotation is 23 ± 6° and the inclination is consistent with the expected value for 0–20 Ma.

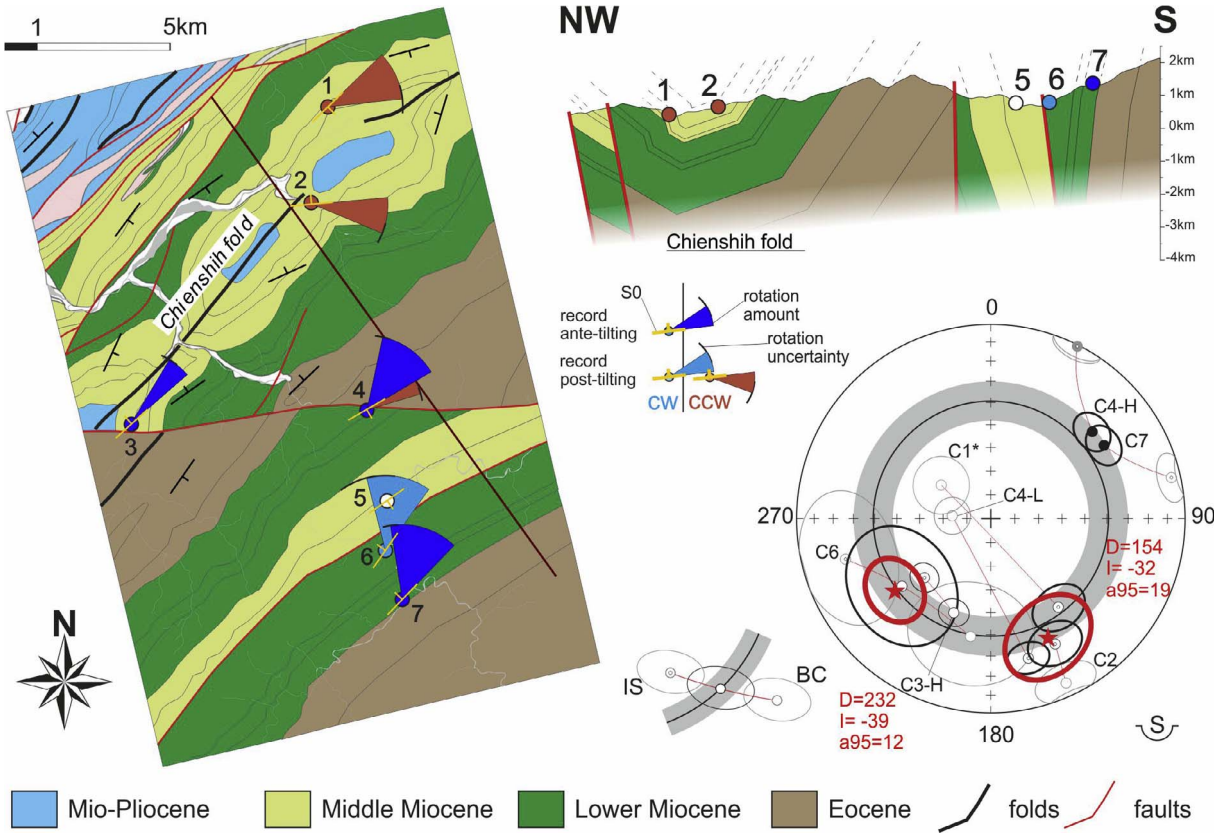

Fig. 13. Results of the analysis of the remanent magnetization for the C-area. Same legend as Fig. 11.

4.3.5. Taichung and Nantou areas (E and F areas)

In the southernmost areas, the E and F areas, half of the components of magnetization show reverse polarity, E3, E2 and F3-H. The numbers of suitable results are too few for performing a pertinent fold test. We thus considered their folding/tilting paths in the stereographic plots and the consistency with the expected inclination for SE Asia (Fig. 15). Some components of magnetization, i.e., E1, E2, F5, exhibit a clear record either before folding/tilting (e.g., F5 and E2) or during folding (e.g., E1). For others, i.e., E3, F2 and F3, the interpretation is not obvious, due to a magnetization which remains consistent with the expected inclination during the course of the back-tilting process. Because the corresponding rotation for E1, E2 and F5 is null or negligible, we favor the configuration which minimizes the declination difference with the corresponding paleomagnetic north trend.

4.3.6. Tatun-Linkou area

The Tatun-Linkou (T-L) area has been sampled previously by Hsu et al. (1966), Horng (2014). The results of Hsu et al. (1966) have been already presented (see Section 2.3). Horng (2014) did not perform statistical analyses of the remanent magnetizations. In this study, we conducted the statistical analyses (Fig. 2) on 1–2 specimens per sites, for a total of 19 specimens. One reverse component of magnetization has been found in each specimen, most of them with good consistency during the demagnetization process and show a quite good grouping. The average magnetization was calculated from 14 components. The resulting magnetization shows a good consistency in declination with the expected values for the 0–10 Ma period. The inclination is consistent, but slightly lower than the expected inclination according to the age of the sampled formation, 1.5–1.2 Ma. The resulting magnetization is consistent with the averaged magnetization for the Tatun volcano group in age of 1.2–0.5 Ma.

4.3.7. Chiaopanshan area

The Chiaopanshan (Ch) area in Taoyuan has been sampled by several previous studies for a total of 30 sites. However, none have been able to obtain an interpretation faithful to the data. We propose here to perform the fold test with the data of magnetizations published by Hsu et al. (1966), Miki et al. (1993) and Lue et al. (1995)(Fig. 16). Our results allow to distinguish two main behaviours (Fig. 9-E): (1) a declination in the SE quadrant, located north to Yuanshan fold axis, and (2) a declination in the SW quadrant, mainly located in the southern limb of the fold. Most of the components show reversed polarity after bedding back-folding correction, except Ty04 being normal. Three Miocene formations, including the Kueichulin, Tungkeng and Mushan formations, have been sampled. Similar to other areas we selected the configuration of magnetization that allows minimizing the difference in inclination with the expected inclination for the 0–20 Ma period. For most sites the position after bedding back-folding is consistent in inclination; on the other hand, the C11-12-13-14, Nt5 and Nt43 propose syn-folding magnetization. We then distinguish three sub-areas according to the homogeneity of the results: (1) the southern area, (2) the north limb of the Yuanshan fold and (3) the northern area.

1. The southern area shows a clockwise rotation of about 15° in the south limb of the Yuanshan fold and up to 63° for Nt10 further south belonging to another thrust sheet. The magnetizations of the south limb of the Yuanshan fold exhibit a very low inclination of 20°.
2. The north limb of the Yuanshan fold presents a clear counterclockwise rotation of about 26° with a consistent inclination of about 40°, although C13 and Nt8 have lower inclinations. We found both syn-folding and ante-folding magnetization at the sites close to the hinge of the Yuanshan fold.
3. The interpretation of this multiple magnetization remains difficult for the northern area with both clockwise rotations carried by ante-folding magnetizations (Nt1 and Ty04), with counterclockwise

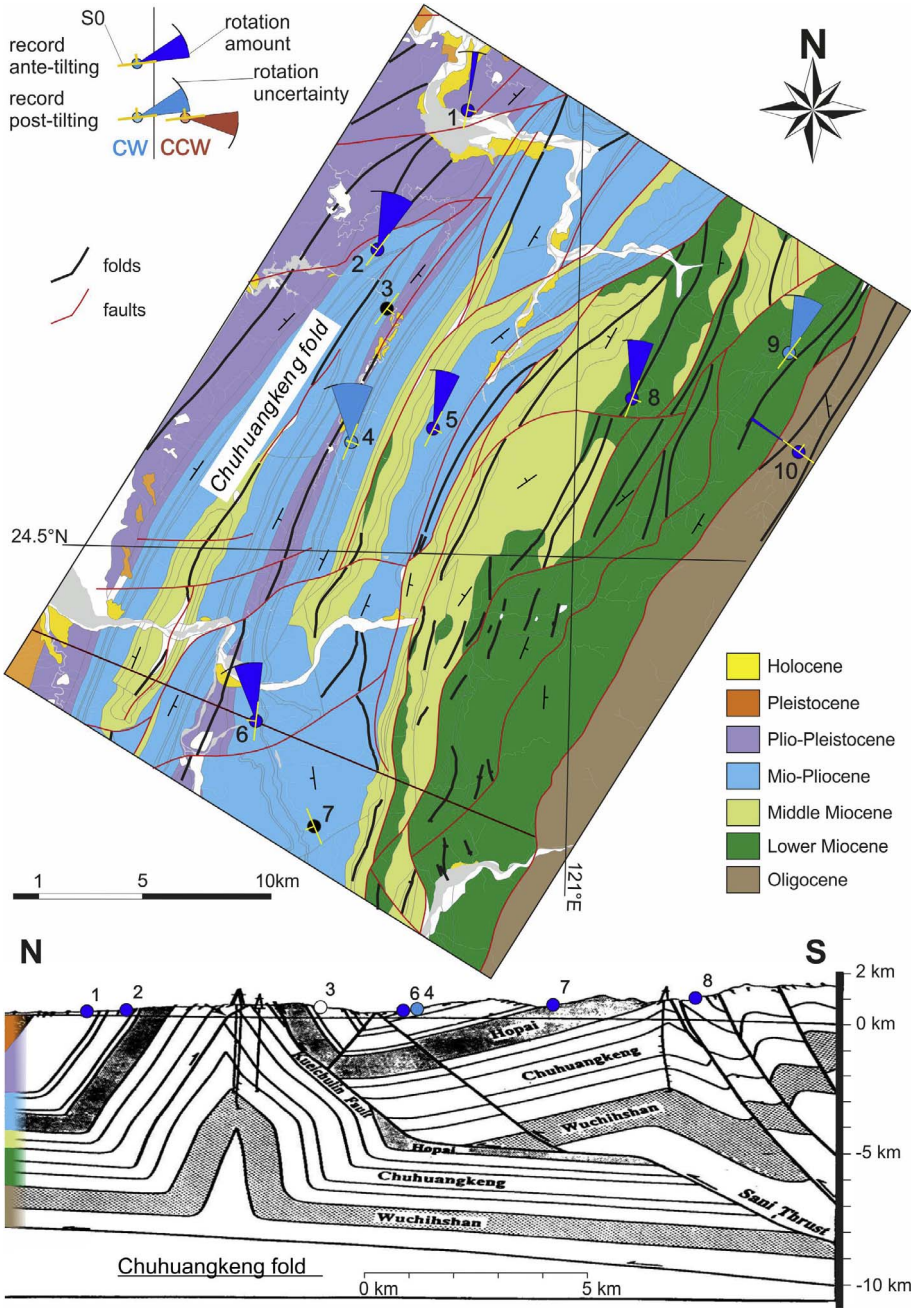

Fig. 14. Results of the analysis of the remanent magnetization for the D-area. Same legend as Fig. 11. The cross-section has been modified from Hung and Wiltschko (1993).

rotations carried by ante-folding (Ty03-05, Nt3-4 and C08-C09) and syn-folding (Nt2-5 and Nt43) magnetizations.

4.3.8. Fei-Tsui reservoir area

The Fei-Tsui reservoir area has been previously sampled by Lee et al. (1991) and Lue et al. (1995), for a total of 14 sites (Fig. 17). We also propose here to perform the fold test with the magnetizations they determined. All the components are reverse and mostly oriented in the SW quadrant, except Ti02 oriented in the SE quadrant. Despite a still poorly fitting grouping, the fold test reveals that the configuration after bedding correction reduces the inclination difference with the expected paleo-inclination as proposed by previous authors.

4.4. Multiple magnetization events and timing

Our paleomagnetic study highlights multiple rotations of different senses and amounts (Fig. 9), especially in the northern half of the North Taiwan Foreland Salient, including the Wanli-Shangchi (A-area), the Taoyuan (B-area), the Chiaopanshan and the Hsinchu (C-area) areas. Others areas present either no rotations, such as the Tatun, Taichung and Nantou (E-F areas) areas, or a single rotation, such as the Keelung, the Miaoli (D-area) and the Fei-Tsui area. In the following sections, we will first distinguish the different components of magnetization before discussing their age of magnetic acquisition and the timing of the corresponding rotations with respect to the folding/tilting of the strata and the structural framework.

4.4.1. The Bruhnes viscous L-components

Compared to previous studies showing single magnetization, most of our sampled sites reveal two components of magnetization. The L-component has low coercivity and low to medium blocking temperature. It is the first one identified in the demagnetization processes. This component is normal polarity with overprint character, thus we interpret to be recorded in the later stage of the mountain building, mostly

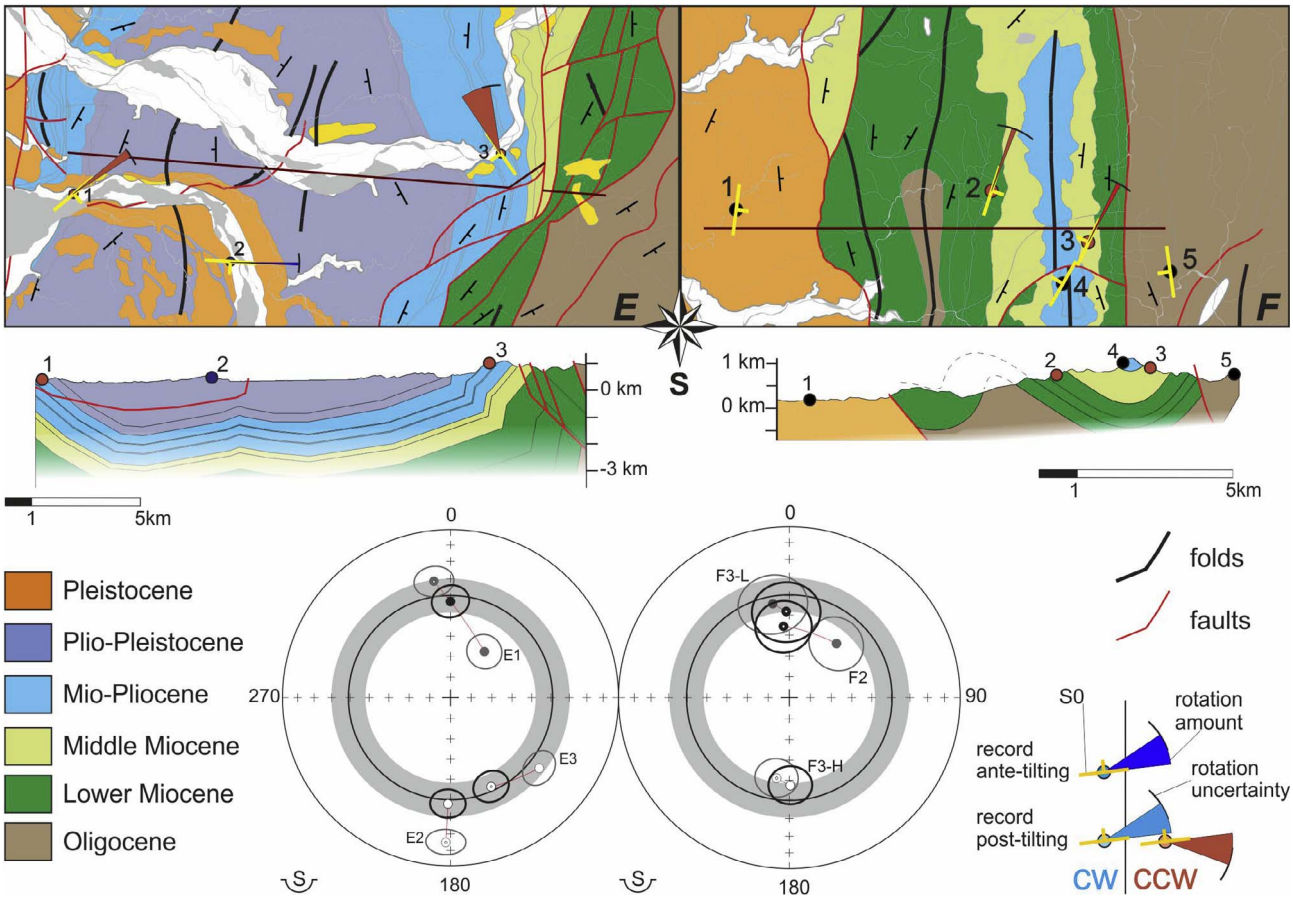

Fig. 15. Results of the analysis of the remanent magnetization for the E and F areas. Same legend as Fig. 11.

after the tilting/folding of the bedding. No significant rotation is associated with it (Fig. 18). The resulting average magnetization is lower in inclination (10 ± 4°) than the expected inclination for SE Asia (Cogné et al., 2013). But the mean L-component magnetization remains in the range of uncertainty of the mean magnetization of the Tatun volcano group (Hsu et al. (1966)), Figs. 2 and 18. As the age of the sampled formations of the Tatun is well constrained, between 1.2 and 0.4 Ma, we interpret the L-component to be a viscous overprint acquired during the Brunhes normal period over the last one million years.

4.4.2. Ages of magnetized components of stable blocks

In this section, we provide possible ages of the magnetizations to the areas showing no significant block rotation, such as the Linkou terraces (=Tatun area), the Keelung and the Taichung and Nantou areas. The Pliocene Tananwan formation in the Linkou terraces presents a reversed magnetization showing good consistency with the expected magnetization during 0–10 Ma (Fig. 18). We can notice that like the common L-components, the average magnetization for the Tananwan formation is slightly lower in inclination especially with the reference magnetization for present time. The L-components are post-tilting so by essence they can be recorded any time after the folding.

Volcanic formations of the Keelung area show normal and reversed magnetizations that can be related to Brunhes and Matuyama period respectively (0.5–1.5 Ma), according to the age of the sampled lava layers and the secular variation records (Hsu et al., 1966).

The sites providing results for the Taichung and Nantou areas reveal both normal and reversed magnetizations. The normal ones are overprints, probably recorded during Brunhes normal period. The reverse ones predates the folding. As we sampled in Plio-Pleistocene (Cholan formation, E2 site) and Middle Miocene (F3 site) rocks, we can attribute the record of the E2 magnetization to Matuyama or Gauss reversed periods. As for the Taichung area, the determination of age in the Nantou area is more challenging as many periods can match with the ante-tilting reverse magnetization of F3 site. The most interesting observations are that three areas, including the southern branch of the NTFS, the Tatun volcanoe and the foreland Linkou terraces, have been the witness of no rotation.

4.4.3. Local block rotations

Among the magnetizations carrying substantial rotation, some of them can be attributed to local structures, such as fold periclinal termination (B4-H and E3), folding with limb opposing rotations (counterclockwise rotation of the northern limb of Yuanshan fold and clockwise rotation of the southern limb). However, some are inconsistent in first order with rotations of surrounding structures (Ti2 and Ti6, Fei-Tsui area). In discussing a broader regional scale structural evolution, these magnetizations have been temporarily discarded for avoiding the local influences not representative at the scale of the NTFS.

4.4.4. Counterclockwise rotations

Among the H-components, we distinguish counterclockwise rotations and clockwise rotations (Fig. 19). From the first glance, we found that many areas, including the Hsinchu (C-area), the Chiaopanshan, the Taoyuan (B-area), the Fei-Tsui and the Wanli-Shangchi (A-area) areas, all exhibit counterclockwise rotations. No specific block rotation can be attributed to these components, except for the north limb of the Chiaopanshan fold. In general these components are recorded after tilting/folding of the strata, except those near the Tahsi thrust and the Chiaopanshan fold. These two areas are next to each other in the foreland. The amount of rotation, from site to site are in the range of −10 to −50°. Despite such large variation, the average rotation remains similar about −30° from south to north for the four areas (i.e., Hsinchu,

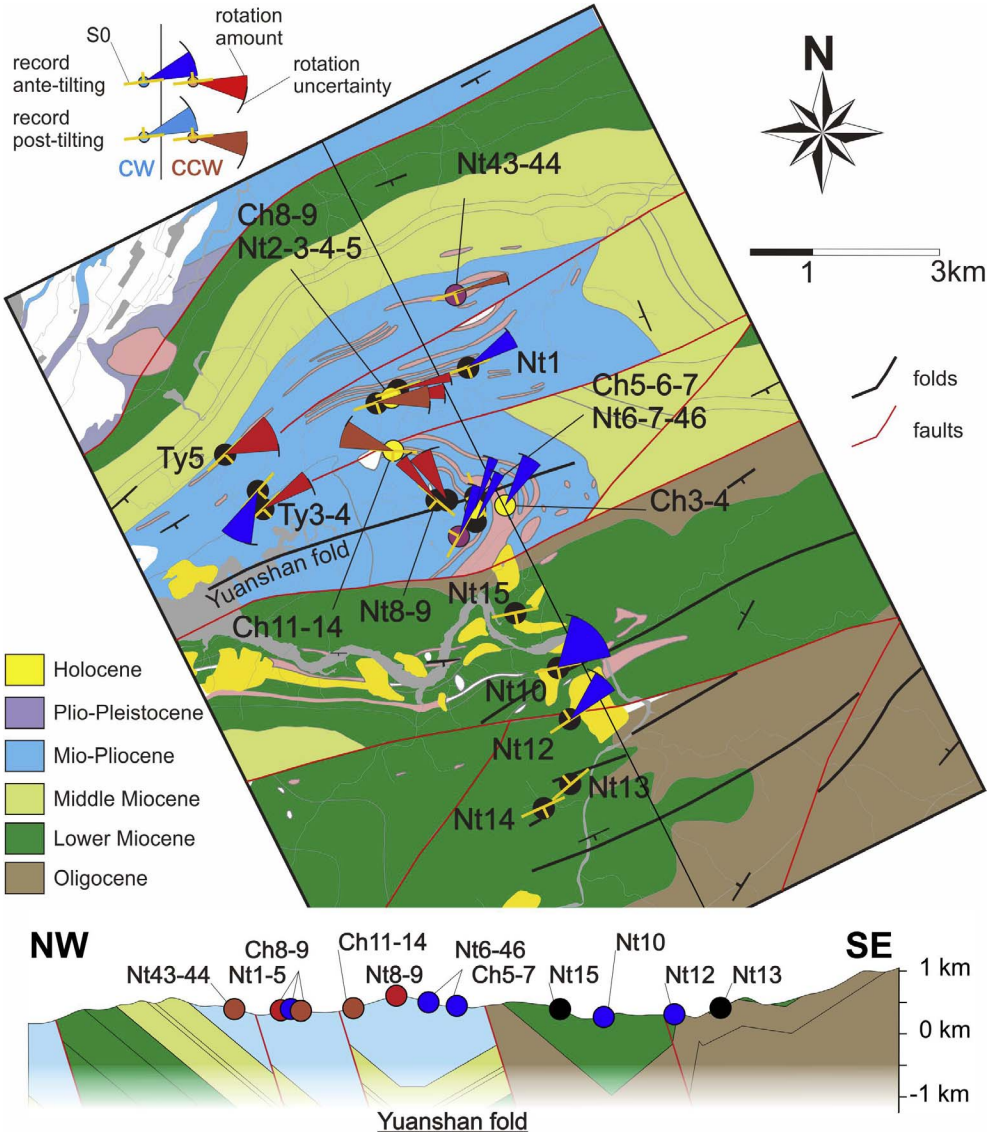

Fig. 16. Results of the analysis of the remanent magnetization for the Chiaopanshan area. Location of the sampled sites are mapped according to the legend of the Fig. 1. Same legend as Fig. 11.

the Taoyuan, the Fei-Tsui and the Wanli-Shangchi areas). No specific distinction can be observed between the Western Foothills and the Hsuehshan Range.

4.4.5. Clockwise rotations

All along the NTFS, the most apparent rotation is the clockwise rotation carried by H-component magnetizations. There are several pieces of evidence for this rotation from South (D area) to North (the Keelung area) (Fig. 19). The fold tests reveal that the clockwise rotation is carried by possible primary magnetizations (recorded before folding/tilting) as well as overprints of secondary magnetizations (recorded during or after folding/tilting).

The consistency between the trend of the bending structures of the NTFS and the amount of rotations favor the interpretation of a regional clockwise rotation increasing toward the north: from 0–10° in the south, to 30–40° in the north. Note that one exception site in the Hsuehshan Range in the Hsinchu area (C area) exhibits strong clockwise rotation about 50°.

5. Discussion

Our study of the paleomagnetic rocks properties along the NTFS points out the existence of multiple records of different remanent magnetizations at different stages of bedding tilting/folding, during exhumation of rocks along the propagation of thrust sheets (Fig. 19). In the following sections we will discuss our tectonic interpretations, by considering the geological context of the North Taiwan Foreland Salient.

5.1. Chronological order of regional block rotations

The fold-test, especially in the Wanli-Shangchi area (i.e., A area), allows to distinguish up to three distinct components of remanent magnetization and to propose the succession of clockwise rotations carried by ante-folding and post-folding magnetizations, followed by a post-folding counterclockwise event. In more details, most areas confirm the existence of a regionally widespread clockwise rotation and the northern half of the NTFS (Hsinchu to Wanli-Shangchi areas) indicates an additional counterclockwise event. Except a few places exhibiting local block rotation, both clockwise and counterclockwise rotations show regional effect as they are homogenously distributed along the NTFS (Fig. 19).

The remaining, challenging questions are the chronological order between these two rotations and which age they correspond. The chronology is not obvious as both rotations are carried by ante-folding magnetizations and post-folding magnetizations, which led to some

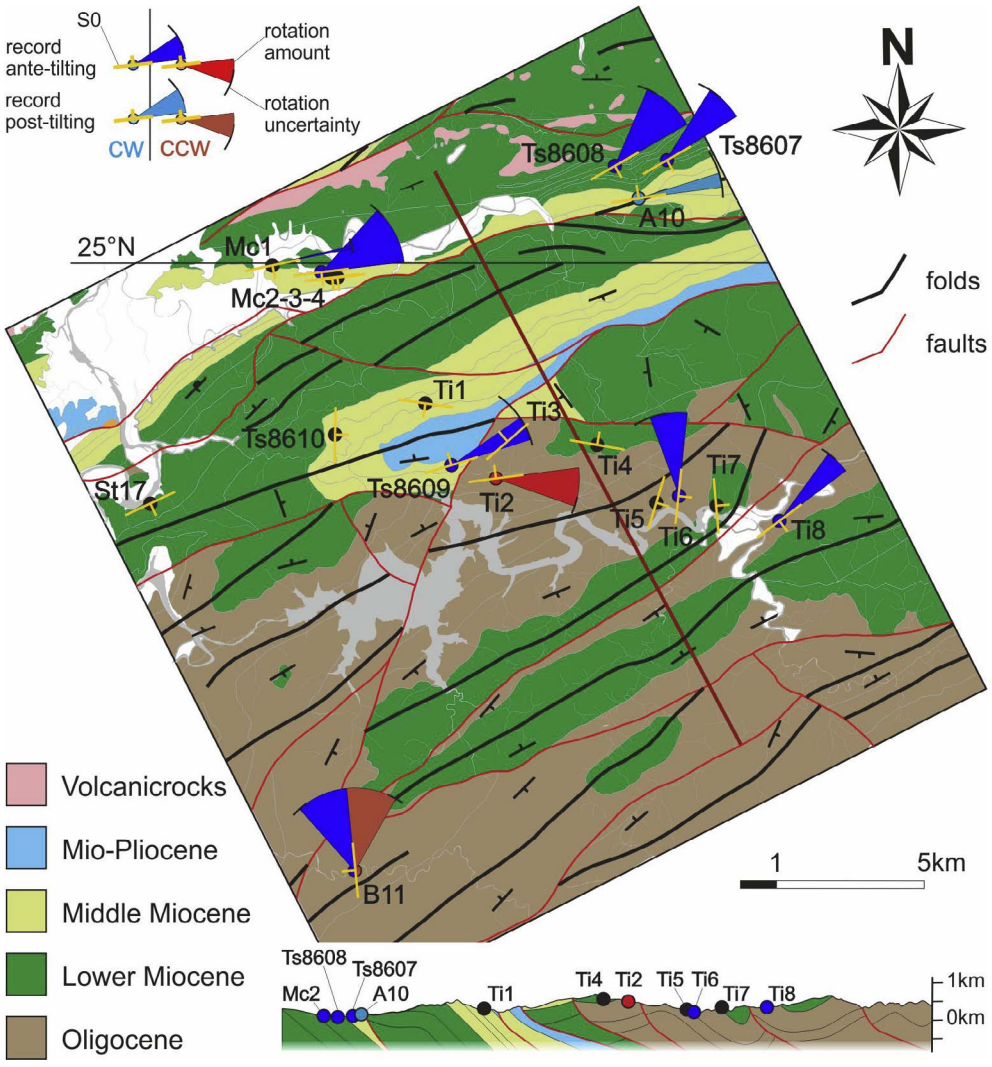

Fig. 17. Results of the analysis of the remanent magnetization for the Fei-Tsui area. Location of the sampled sites are mapped according to the legend of the Fig. 1. Same legend as Fig. 11.

misinterpretations by Lue et al. (1995) and Sonnette (2012). No structural relation can be obviously observed because the samples are located usually among tectonic units parallel to each other. Note that our aforementioned main argument about the relative chronology between clockwise and counterclockwise rotations at sample scale is based on 4 sites: A23, B4, B11 and C4. For these sites, the components carrying the counterclockwise rotation are always demagnetized before the components carrying the clockwise rotation which suggest that the counterclockwise rotation postdate the clockwise rotation. About the regional coverage of the different rotations (Fig. 19), the counterclockwise rotations, which are carried by ante-folding magnetization, are restricted to the Chiaopanshan and Taoyuan areas. By contrast, the clockwise rotations carried by ante-folding magnetization are widespread in the whole NTFS. These two arguments support the argument that a regional clockwise rotation is followed by a regional counterclockwise rotation.

5.2. Amount of rotations

Because of these multiple, successive rotations, the chronology of the regional rotations indeed provides great help on estimating the net amount for each regional rotation event. As several areas have experienced both counterclockwise and clockwise rotations and the clockwise rotation occurred before the counterclockwise rotation, the net amount of clockwise rotations has to be corrected from the amount of counterclockwise rotations (Table 2). In consequence we obtain the net clockwise rotations amounts in the whole NTFZ, which increase from south to north:

1. 0–10° in the Taichung and Nantou areas;
2. 30° in the Miaoli area;
3. 40–50° in the Hsinchu-Chiaopanshan-Taoyuan areas;
4. up to 60–70° in the Fetsui-Wanli-Shangchi areas.

Such pattern reveals a strong correlation with the regional bedding strike and main structures orientations along the NTFS. It thus corresponds to an oroclinal bending process (Schwartz and Van der Voo, 1983; Yonkee and Weil, 2010). One can also notice for the Hsinchu area that the corrected clockwise rotation in the Western Foothills (outer part) is the same as in the Hsuehshan range (inner part of the NTFS).

5.3. Primary magnetizations versus overprints

The post-folding magnetizations are secondary magnetizations or overprints. By contrast, ante-folding magnetizations can be primary magnetizations or overprints. For the magnetizations carrying either the clockwise or counterclockwise rotations, the overrepresentation of reversed polarities argues for overprinting magnetization. For the samples showing ante-folding normal magnetizations with counterclockwise rotation, they are all located in the Kueichulin formation (3.5–6.5 Ma) for which the probability to record a reverse primary magnetization is around 75%. The fold-test favors an ante-tilting record

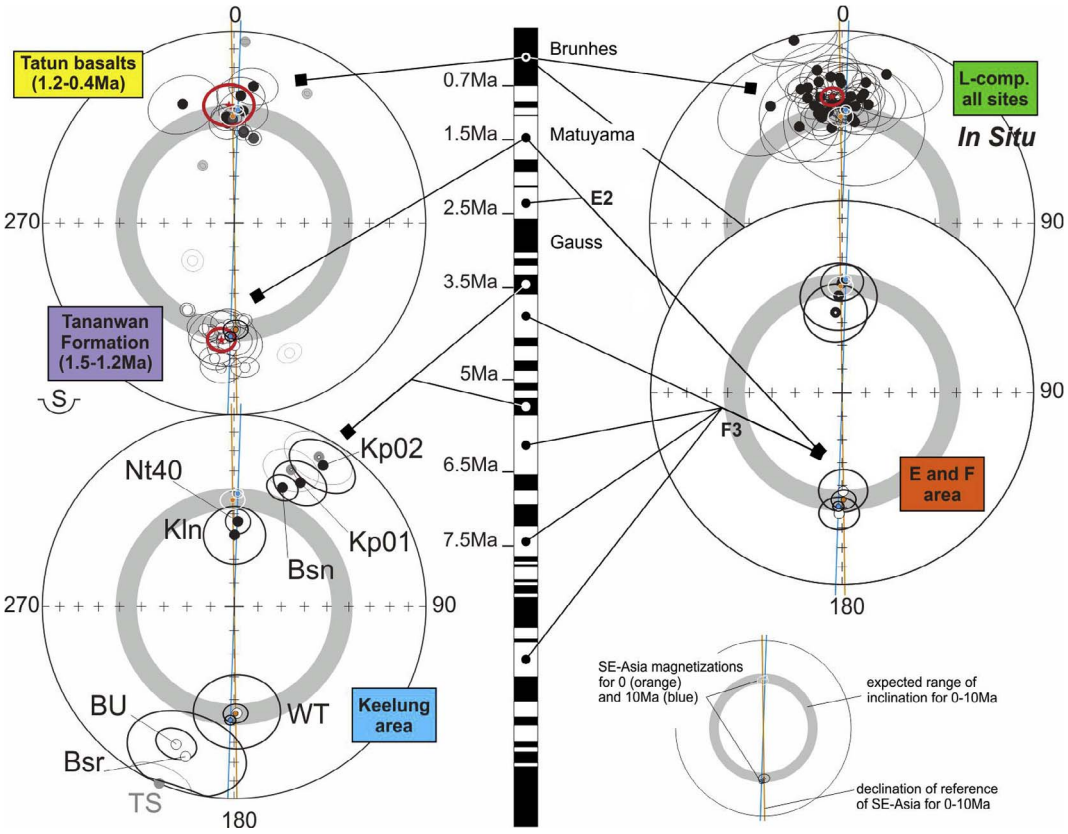

Fig. 18. Interpretation of the L-components regarding the polarity and the results for the youngest formation. The L-components are compared with the results for the basalts of the Tatun volcano and the Keelung, the sediments of the Tananwan formation, and the sites of the E and F area. The grey circle correspond to the expected inclination for SE-Asia at the locality of Taipei for the 0–10 Ma period. The magnetostratigraphic scale of reference is represented by the succession of black and white rectangles.

but it is not significant enough to exclude the possibility of an overprinted magnetization during the early stage of tilting/folding (e.g., 10% of tilting). As a result we cannot rule out the counterclockwise ante-folding magnetizations in the Kueichulin formation being overprints, although it is less likely. Nevertheless, the clockwise ante-folding magnetizations provide more determinant clues. These magnetizations are recorded rock formations in a large range of age. The quality of the signals does not allow us to clearly evoke primary

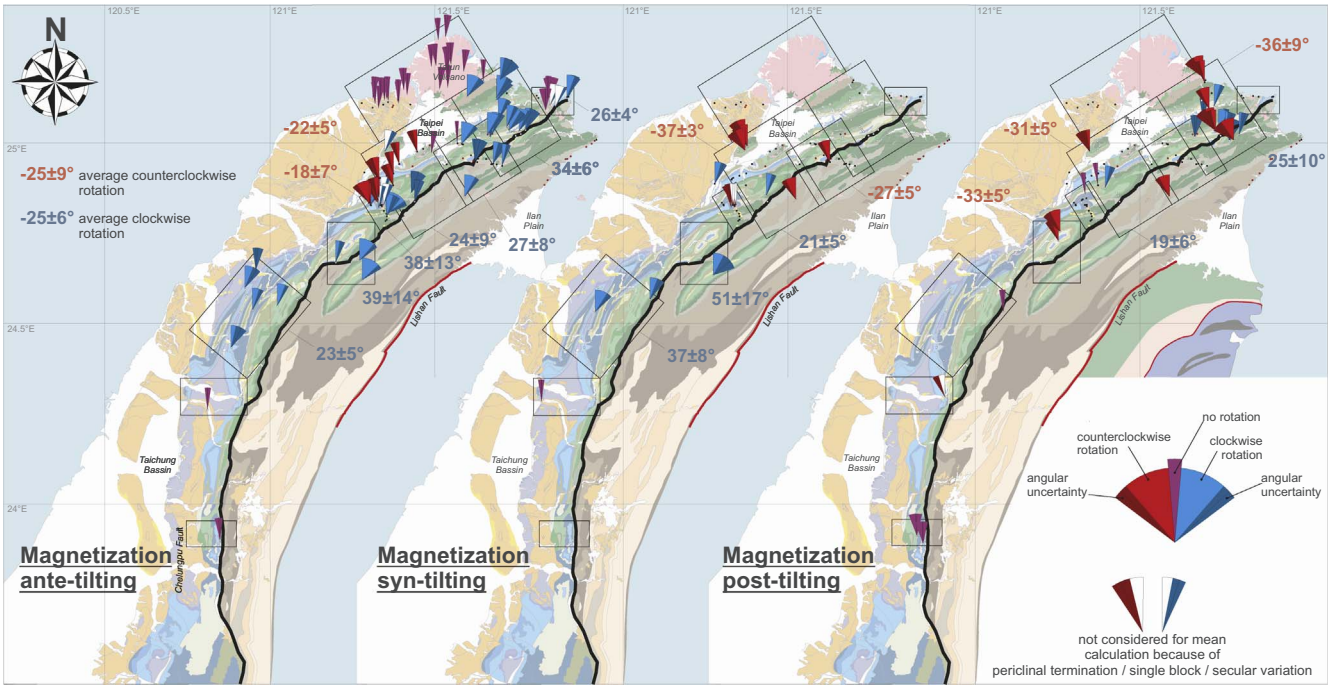

Fig. 19. Synthetic maps showing the amount and sense of rotations for the ante-tilting, syn-tilting and post-tilting magnetizations from left to right. The thick black line corresponds to the boundary between the Western Foothills and the Hsueshan Range.

Table 2
Synthesis of the paleomagnetic results along the NTFS. Average amount of rotations are provided by area and according to the age of the sampled formations. The numbers in brackets refer to number of results used for the calculation of the corresponding average. All the angles are expressed in degrees.

	Age sampled formation	Taichung and Nantou	Miaoli	Hsinchu	Chiaopanshan	Taoyuan	Fei-Tsui	Tatun	Wanli-Shangchi	Keelung
		E-F area	D area	C area		B area			A area	
Foreland	Post 1.5 Ma	–	–	–	–	–	–	0 (>20)	–	0 (3)
	Cholan (1.1–2.6 Ma)	0 (1)	6 ± 11 (1)	–	–	–	–	–	–	–
Western	Kueichulin (post-folding)	–	41 ± 7 (1)	–	–	–	–	–	–	–
Foothills	Kueichulin (ante-folding)	0 (1)	31 ± 3 (2)	–	–	−22 ± 5 (6)	–	–	–	26 ± 4 (2)
	Ante 6.5 Ma (post-folding)	–	–	−33 ± 5 (2)	−18 ± 7 (6)	−35 ± 4 (6)	−31 ± 4 (2)	–	−36 ± 9 (6)	–
	Ante 6.5 Ma (post-folding)	–	32 ± 9 (1)	–	–	20 ± 2 (2)	–	–	25 ± 10 (8)	–
	Ante 6.5 Ma (ante-folding)	0 (2)	25 ± 2 (2)	18 ± 6 (1)	38 ± 13 (4)	23 ± 3 (2)	–	–	34 ± 6 (12)	–
Hinterland Hsueshan Range		–	0 (1)	50 ± 2 (3)	–	37 ± 6 (1)	27 ± 7 (3)	–	26 ± 8 (4)	–

magnetization, as demagnetizations rarely cross the origin in Zijderveld diagrams. Also the impossibility to lead a reversal test due to very few numbers of samples with normal polarity does not support the existence of some true primary magnetizations. The reversed polarities definitely argues for overprinting magnetizations as the potential period for primary magnetizations extends over 20 Ma.

Magnetization overprinting can be due to different processes, including burying and deformation processes. Most of the sampled sites were in non-metamorphic rocks, which had not encountered temperature over 200 °C (Chen et al., 2011). It corresponds to the thermal window of formation of magnetite proposed by Aubourg et al. (2012). In clay or shale, the sole action of temperature leads to the formation of chemical remanent magnetization of magnetite. The ante-folding magnetization can be this kind of overprint recorded during the burial of the rock formations. In addition overprints can be the results of orogenic fluid or pressure solution (Elmore et al., 2001; Elmore et al., 2006; Aubourg et al., 2008). All sites with overprint H-components are associated with a regional fold (A15-16, B1-2-3, C2 and D4-9) or a major fault (A7-8-19-21-22-23-24, B6-10 and C6-11-14). Further geochemical analyses are required to confirm such speculations.

5.4. Ages of magnetizations carrying counterclockwise rotations

Ante- and post-folding magnetizations, which reveal counterclockwise rotation, are interpreted as H-component; and they would be older than the L-components. As previously described, the age of L-components can be defined, either younger than 1.5 Ma for most of them, or younger than 2.5 Ma for others (Fig. 18 and 4.4.1). The ante-folding counterclockwise magnetization have been recorded either during the Kueichulin formation deposit (6.5–3.5 Ma) as primary magnetization or at the initiation of the folding, as overprint, which probably occurred after 3.5 Ma. The post-folding magnetizations which experienced counterclockwise rotations afterward have been recorded during a reverse period between 3.5 and 1.5 Ma. The knowledge of the age of folding would allow reducing this time range. Since most of the folding is closely associated with major thrusting (either fault-bend fold or fault propagation fold), the timing of major thrusting can be adopted for age estimation. As a consequence, we used the following constrains of timing for the collision in the NE Taiwan:

1. the formation of the Ilan plain due to the opening of the Okinawa Trough determined around 2–2.8 Ma and;
2. the onset age of the molasses of the Toukoshan formation (e.g., Linkou conglomerate) of about 2 Ma.

Following the hypothesis of the collapsing of the orogen in NE Taiwan (Teng and Lee, 1996), it is a general assessment that the thrust and fold structures were mostly formed around 2–3 Ma. Immediately after 2.5 Ma until 1 Ma, there are a long reversal, from 1.9 to 2.6 Ma, suitable for the record of the counterclockwise post-folding magnetization.

5.5. Ages of magnetizations carrying clockwise rotations

In the NE of the NTFS, among the same structures, our results show evidence of significant clockwise rotations carried by both ante-folding and post-folding magnetizations (Fig. 20 and Table 2). The amount of rotations of the clockwise rotations are similar whatever the timing magnetization records and whatever their location in the foreland or the hinterland. The straightforward interpretation would be that the clockwise rotation occurred after the folding/tilting of the bedding like the counterclockwise rotations. It will also imply that only faulting-related rotation, without any significant regional folding, would explain such rotational pattern (i.e., clockwise then counterclockwise rotations), once the NTFS was developed. The folding/tilting of the bedding is unambiguously related to the formation of fold and thrust belt or the NTFS here. To make a proper interpretation it is necessary to consider the way of folding. The NTFS was developed by propagation and stacking of thrust sheets soliciting some inherited normal faults. Such way of deformation generated sometimes asymmetrical folding, or tilting of the different limbs at different rates and amounts. Thus it is possible to interpret the mixing of ante- and post-folding magnetizations as a single syn-folding magnetization event. In Fig. 20, we propose the geometry of the Wanli and Pinxi folds in the A-area when could have occurred the syn-folding magnetizations.

As a consequence, the magnetizations carrying clockwise rotation would be recorded during the regional folding of the NTFS, and then a significant lateral variation of clockwise rotation would occurred from 0° in the SW, 20–30° in the middle, to 60–70° in the NE. It can be proposed that the NTFS was developed in two steps:

1. initiation of thrusting and related folding and,
2. progressive clockwise rotation from SW to NE and termination of folding.

Moreover, the samples within the upper Kueichulin formation in the Keelung area (Nagel et al., 2013, 4.6 Ma) indicate that it is the youngest formation where ante-tilting magnetizations has been recorded. In the Miaoli area, the rotation is recorded after the deposit of the Kuechulin

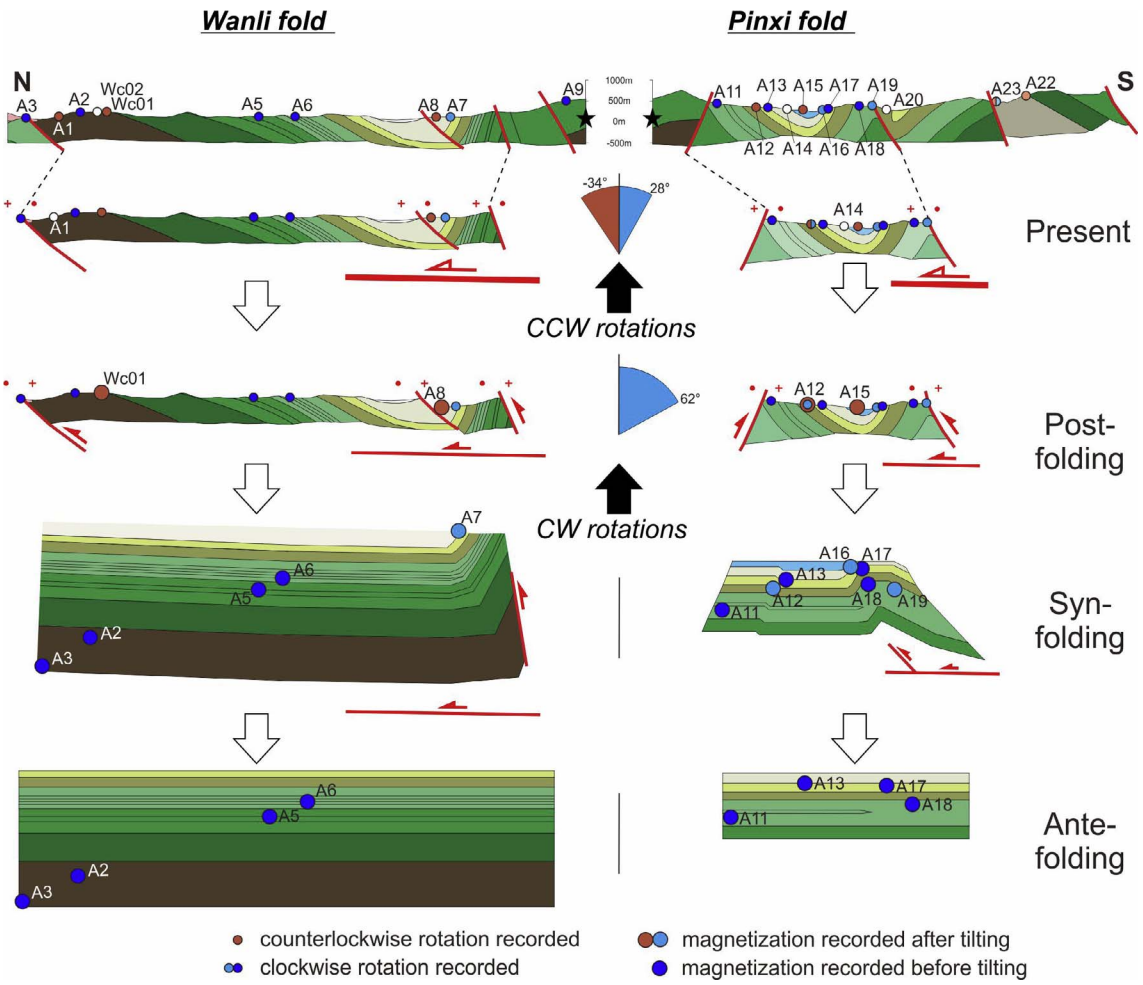

Fig. 20. Synthetic restoration of the Wanli and Pinxi folds (A-area in Fig. 1). The location and timing of the magnetization record are represented. The activity, thrusting or strike-sliping, of the main faults is proposed in order to accommodate the counterclockwise and clockwise rotations respectively. Ante-folding magnetization are assumed to be recorded either before any deformation process or during folding. Post-folding magnetization carrying clockwise rotation are assumed to be recorded during folding (see Section 5.5 for further explanations).

formation, around 3.5 Ma, as suggested by the post-folding magnetizations record. The rotation continued to occur even after 2.6 Ma, as the clockwise rotation is recorded in the Cholan formation. For the NE part of the NTFS, the clockwise rotation stopped probably around 2.5 Ma when the Ilan Plain started to be affected by the opening of the offshore Okinawa Trough, whereas it stopped about 1.1 Ma in the SW part of the NTFS. These timings are quite consistent with the fact that a decrease of clockwise rotations are found from NE to SW as the collision lasted longer in the NE than the SW of the NTFS (Fig. 21). We propose that the 30° in SW (i.e., Miaoli) and 60–70° clockwise rotations in NE (i.e., Wanli-Keelung) occurred during 1.1–3.5 Ma and 2.5–4.6 Ma, respectively.

5.6. Plan view restoration of the NTFS

The paleostress analysis carried out by Angelier et al. (1990b) proposed 4–5 main tectonic episodes, which have then been reduced to 2 major events by Chu et al. (2013). However, it remains difficult to date the tectonic events within the NTFS because syn-collisional sedimentary formations are restricted to the southern part of the salient. In such context, the characterization of a tectonic event is mainly based on comparison of the results of main tectonic compression directions from one site to another. But in the case where significant rotations are expected, the apparent complexity of fracture sets can be the result of a single tectonic event recorded several times during the rotation (Allerton, 1998). Considering the rotational pattern of the NTFS it might worth to examine again the results of Angelier et al. (1990b), in order to better describe the evolution of the compressive direction during the genesis of the NTFS.

In the NE part of the NTFS, from youngest to oldest, Angelier et al. (1990b) proposed the distinction of N150E, N110E and N180E trending subsequent compression events. In the hinge of the NTFS, they proposed N140°E, N110°E and N170°E trending subsequent compression events. In the SW part of the NTFS, they proposed only two subsequent events of N110°E and a N130°E trending compression. It is worthy to notice that among the youngest, intermediate and oldest events the angular deviation is:

1. about 40° counterclockwise followed by 70° clockwise changes in the NE part;
2. about 30° counterclockwise then 60° clockwise changes for the hinge zone and
3. about 20° clockwise change in the SW part. These different amounts of changes of compressive direction, in particular the clockwise change, are consistent to the net amounts of clockwise rotations we obtained from paleomagnetic studies for the different areas.

So, as a first attempt, we tried to correct these paleostress directions by using our paleomagnetic rotational pattern (Fig. 21). Because the youngest compression direction in the SW area is parallel to the current GPS shortening direction, it is not affected by any rotations. We assume that all the youngest compression events occurred after the regional

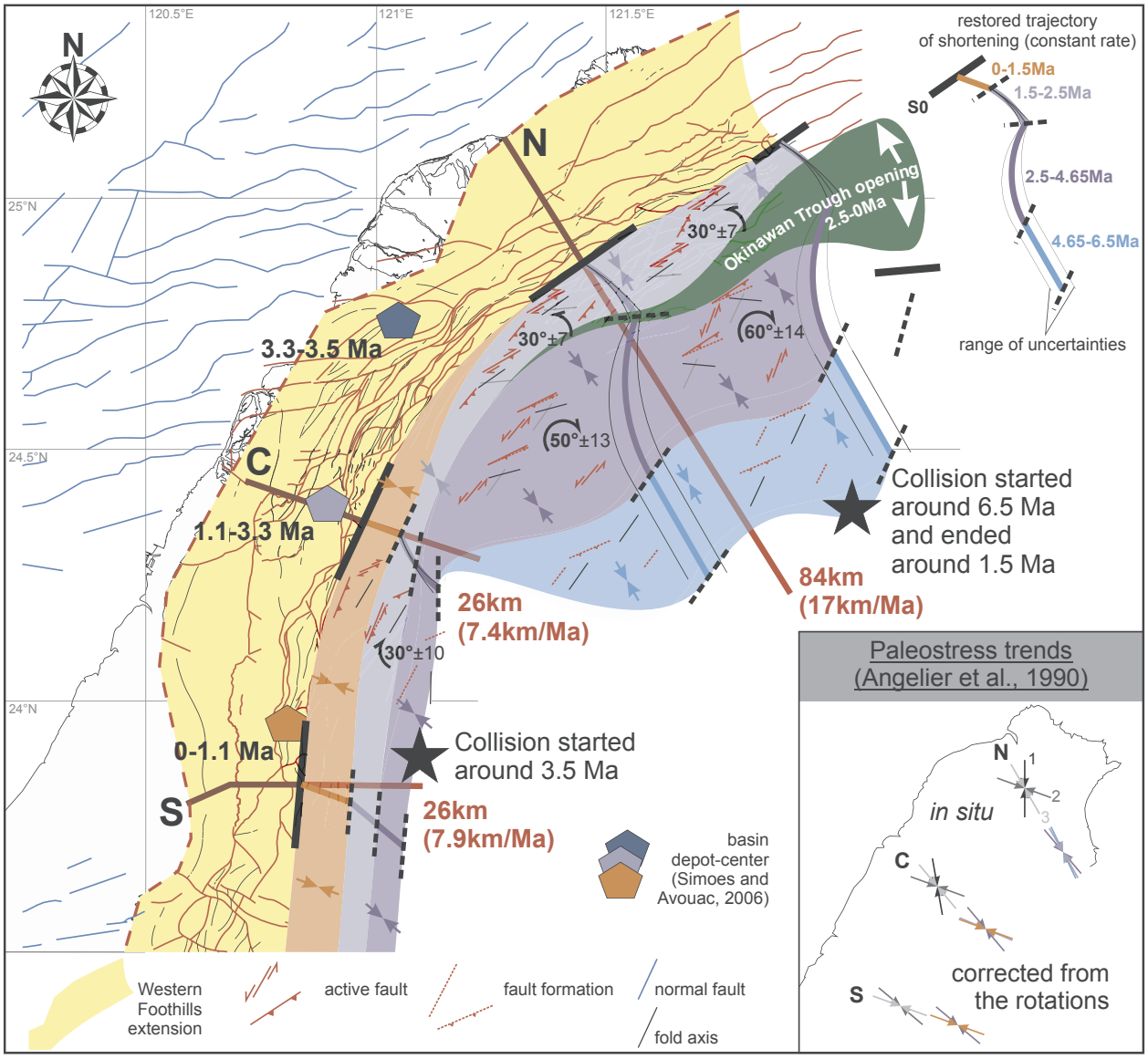

Fig. 21. Synthetic trigonometric model restoring the extension of the Western Foothills during the collision. For explanation see the Sections 7.6 and 7.7.

block rotations. It is thus possible to explain all these different events of compressive directions in a rather simple frame, N140–150°E from 6.5 Ma to 1.5 Ma and N110°E from 1.5 Ma to present, making the NTFS a nice example of the prediction of the Allertons model (1998). It is also interesting to notice that the correction of the paleostress trends propose an initial N140–150°E consistent with the trend of the stretching lineation, N325°E, in the Central metamorphic belt (Faure et al., 1991).

Unlike the paleostress determination showing complexity, the general trend of the bedding strikes, fault traces and fold axes, remains always parallel to each other all along the NTFS from south to north. This pattern could be the expression of the inherited structures of the Chinese continental margin dominated by ENE-WSW and NE-SW faults Chen and Watkins (1994), Lin et al. (2003). This pattern would be solicited either as reverse faulting or strike-slip faulting depending on the accommodation of clockwise or counterclockwise rotations (Fig. 21) as shown by structural analysis of Lu et al. (1995). Combining the consistency between the orientations of faults and bedding strike and in close relation with clockwise rotations, it all indicated that the gradually increasing amounts of clockwise rotation toward the NE of the NTFS is mainly produced by horizontal bending occurred coevally with folding and thrusting during the mountain building. So we interpret such bending as the manifestation of progressive rotation by extrusion rather as a pure oroclinal bending.

Several geologists made balanced geological cross-section along the NTFS (Suppe, 1986; Hung and Wiltschko, 1993; Yue et al., 2005, for sections N, C and S respectively in Fig. 21). By adopting their geological cross-sections, we propose a simple preliminary way to reconstruct the propagation trajectories of the particle in the Western Foothills at different steps of development of the fold-thrust belt. Retro-deformation and restoration of a fold-and-thrust belt is a hard task that required further rigorous work to develop a reliable trigonometric model (Sussman et al., 2012). As the horizontal shortening can be obtained along direction perpendicular to the main structural grains, we estimate the shortening trajectories shown by curved paths. Each curved path is defined by an arc length equal to the estimated horizontal shortening (deduced from the balanced cross-section) and by an arc central angle equal to the determined vertical axis rotation. Once we have defined the different curved trajectory of shortening, we assume that the initial transport was parallel to the direction of compression corrected from the corresponding rotation.

Finally, the readers have to keep in mind that our restoration of the extension of the Western Foothills only take into account balanced geological cross-sections, rotation amounts and paleostress trends. The way of exhumation of the Central metamorphic belt or the motion of

the Philippine Sea Plate on the last 10 Ma are not considered. Lee et al. (2015) reveal that the exhumation of the green schist facies started around 5–6 Ma all along the Taiwan mountain belt which suggest that the collision was simultaneous between north and south Taiwan. In first view such evidence seems incompatible with our interpretation which corroborates a progressive propagation of the deformation from NE to SW. The key points to solve this issue are the knowledge of the exhumation rates and the shortening rates all along the NTFS. Acting for a simultaneous start of the collision, it is necessary to consider different shortening rates to explain the significant change of shortening amount between sections N and C (Fig. 21), the propagation to the south of the clockwise rotations and the progressive regression to the south confirmed by Nagel et al. (2013).

5.7. Bending of the NTFS

The paleomagnetic study of the NTFS reveals the succession of a major regional clockwise rotation then a minor regional counterclockwise rotation from 4.6 Ma to 1.5 Ma. The clockwise rotation with a progressive increase of the amount of rotation from 30° in the SW (Miaoli area) to 60° in the NE (Keelung area) is in good agreement with the curvature of the strata and main structures in the NTFS. We conducted a preliminary restoration of paleo-bedding strikes, back to the initiation of the collision, based on the rotation results of our paleomagnetic study and associated chronology (Fig. 21). The restoration of the latest counterclockwise rotations proposes a general trend of the NTFS similar to the current trend of the Central Range. Supported by present-day kinematic data and seismotectonic stress analyses, Rau et al. (2008) showed a strong clockwise rotation in the southern part of the Ilan Plain and the north-easternmost part of the Central Range. Their results suggested that the southward opening of the Okinawa Trough plays an important role on clockwise rotation south of the Ilan Plain, but counterclockwise rotation north of the Ilan Plain. We follow similar scenario of tectonic extrusion to explain the clockwise rotation pattern along the NTFS. Before the formation of the Ilan Plain, 2.5 Ma ago, there was no back-arc opening process, only plate indentation of the PSP to the CCM. The indentation apparently caused strong progressive clockwise rotation at the plate corner, particularly in the northeastern Taiwan.

The counterclockwise rotations, from the Keelung area to the Hsinchu foreland area between 2.5 and 1.5 Ma seems obviously related to the formation of the Ilan Plain due to the opening of the Okinawa Trough. However, the opening of the Okinawa Trough is controlled by the motion to the South of the Ryukyu Arc (Shinjo et al., 1999) and normal faulting is dominant in the NE Taiwan, offshore (Hsiao et al., 1999) and within the Ilan Plain (Kang et al., 2015). Our data suggest that foreland deformation could be accentuated by extensional process within the Ilan Plain. We interpret the counterclockwise rotations as the manifestation of an oroclinal “un”-bending in response to the opening of the Okinawa Trough.

6. Conclusions

This study presents a detailed paleomagnetic data set, which shows a general consistency between the orientation of the regional structural grain (bedding strike and thrust) and the rotation amounts carried by the remanent magnetizations although the reliability of some sites can be questioned. The sampling in the whole North Taiwan Foreland Salient (NTFS) has been conducted for the first time. The paleomagetic analyses allowed to improve our understanding of the rotational pattern in the fold-thrust belt of a curved mountain belt, based on the seemingly complicated relationships between the multiple magnetizations and the propagation of thrust sheets and the associated folding/tilting of strata during different stages of rock exhumation. We bring both evidence and explanations for the clockwise and counterclockwise rotations thanks to the fold test, and especially of the tilting trajectory of the bedding. We were able to propose a succession of regional rotations for the whole NTFS: first a clockwise rotation during the propagation and stacking of the thrust units, followed by a counterclockwise rotation locally developed adjacent to the northern margin of the Ilan Plain, which is likely synchronous with the opening of the Okinawa Trough. The results of this study can be summarized as followings.

1. The sedimentary formations of the NTFS show weak concentration of magnetic minerals dominated by soft coercivity (less than 0.5 T) mixture of magnetites. By either thermal or AF demagnetization protocol it is hard to reveal characteristic magnetizations (ChRM) due to the weakness of the signal and the presence of superparamagnetic minerals. It would explain why the paleomagnetic analyses present such important uncertainties and their reliability remain questionable in some cases.
2. Major clockwise rotations recorded by multiple magnetizations show increasing amounts of 0° to 60 ± 14° from SW to NE in the NTFS.
3. The magnetizations showing clockwise rotations are recorded either during the ante-tilting or post-tilting stages in response of regional folding, suggesting that they are overprints recorded during the propagation and exhumation of the different thrust sheets.
4. We argue that the clockwise rotations of sedimentary strata occurred between 4.6 Ma and 2.5 Ma in the NE part of the NTFS and between 3.5 Ma and 1.1 Ma in the SW part.
5. Furthermore, we also found a 30 ± 7° counterclockwise rotation only in the NE part of the NTFS and it occurred during 2.5–1.5 Ma, which we tend to interpret it as a result of the northward opening of the Okinawa Trough.

Acknowledgement

The first author deeply appreciates Prof. Jacques Angelier who supervised him during his Ph.D thesis and supported him to study the NE of Taiwan before passing away in January 2010. This study was part of the Doctorate thesis of the first author at the University of Nice Sophia-Antipolis. We are grateful to Academia Sinica for providing postdoc fellowship to the first author, so that the completion of this study would be possible. The first author is also grateful to the University of Corsica for providing a teaching and research position, so that the completion of the manuscript would be possible. This is a contribution of Institute of Earth Sciences, Academia Sinica (IESAS-2157).

References

Allerton, S., 1998. Geometry and kinematics of vertical-axis rotations in fold and thrust belts. Tectonophysics 299, 15–30.
Angelier, J., Barrier, E., Chu, H.T., 1986. Plate collision and paleostress trajectories in a fold-thrust belt: the Foothills of Taiwan. Tectonophysics 125, 161–178.
Angelier, J., Bergerat, F., Chu, H.T., Juang, W.S., Lu, C.Y., 1990a. Paleostress analysis as a key to margin extension: the Penghu Islands, South China Sea. Tectonophysics 183, 161–176.
Angelier, J., Bergerat, F., Hao-Tsu, C., Teh-Quei, L., 1990b. Tectonic analysis and the evolution of a curved collision belt: the Hsüehshan range, northern Taiwan. Tectonophysics 183, 77–96.
Aubourg, C., Pozzi, J., Janots, D., Sahraoui, L., 2008. Imprinting chemical remanent magnetization in claystones at 95 °C. Earth Planet. Sci. Lett. 272, 172–180.
Aubourg, C., Pozzi, J.P., Kars, M., 2012. Burial, claystones remagnetization and some consequences for magnetostratigraphy. Geol. Soc. Lond. Spec. Publ. 371, 181–188.
Biq, C., 1966. Tectonic styles and structural levels in Taiwan. In: Proceedings of the Geological Society of China, pp. 3–9.
Biq, C., 1972. Dual-trench structure in the taiwan-luzon region. Proc. Geol. Soc. China 15, 65–75.
Bowin, C., Lu, R.S., Lee, C.S., Schouten, H., 1978. Plate convergence and accretion in Taiwan-Luzon region. AAPG Bull. 62, 1645–1672.
Byrne, T., 1998. Pre-collision kinematics and possible modern analogue for the Lichi and Kenting melanges, Taiwan. J. Geol. Soc. China 41, 535–550.
Carey, S.W., 1955. The orocline concept in geotectonics-part I. Papers Proc. Roy. Soc. Tasmania 89, 255–288.
Chai, B.H., 1972. Structure and tectonic evolution of Taiwan. Am. J. Sci. 272, 389–422.

Chemenda, A., Yang, R., Hsieh, C.H., Groholsky, A., 1997. Evolutionary model for the Taiwan collision based on physical modelling. Tectonophysics 274, 253–274.
Chen, C.T., Chan, Y.C., Lu, C.Y., Simoes, M., Beyssac, O., 2011. Nappe structure revealed by thermal constraints in the Taiwan metamorphic belt. Terra Nova 23, 85–91.
Chen, T., Watkins, J., 1994. Structure and stratigraphy of South Pengchiahsu Basin, northern offshore Taiwan. Petrol. Geol. Taiwan 29, 127–170.
Chou, J., 1973. Sedimentology and paleogeography of the upper cenozoic system of western Taiwan. In: Proceedings of the Geological Society of China, pp. 111–143.
Chu, H.T., Lee, J.C., Bergerat, F., Hu, J.C., Liang, S.H., Lu, C.Y., Lee, T.Q., 2013. Fracture patterns and their relations to mountain building in a fold-thrust belt: a case study in NW Taiwan. Bull. Soc. Géol. France 184, 485–500.
Clift, P.D., Lin, A.T., Carter, A., Wu, F., Draut, A.E., Lai, T.H., Fei, L.Y., Schouten, H., Teng, L., 2008. Post-collisional collapse in the wake of migrating arc-continent collision in the Ilan Basin, Taiwan. Geol. Soc. Am. Spec. Papers 436, 257–278.
Cogné, J., 2003. Paleomac: a Macintosh™application for treating paleomagnetic data and making plate reconstructions. Geochem. Geophys. Geosyst. 4.
Cogné, J.P., Besse, J., Chen, Y., Hankard, F., 2013. A new late Cretaceous to Present APWP for Asia and its implications for paleomagnetic shallow inclinations in Central Asia and Cenozoic Eurasian plate deformation. Geophys. J. Int. 192, 1000–1024.
Covey, M.C., 1984. Sedimentary and tectonic evolution of the western Taiwan foredeep. Petrol. Geol. Taiwan.
Day, R., Fuller, M., Schmidt, V., 1977. Hysteresis properties of titanomagnetites: grain-size and compositional dependence. Phys. Earth Planet. Inter. 13, 260–267.
Demarest, H.H., 1983. Error analysis for the determination of tectonic rotation from paleomagnetic data. J. Geophys. Res.: Solid Earth (1978–2012) 88, 4321–4328.
Dunlop, D.J., 2002. Theory and application of the Day plot (M_{rs}/M_s versus H_{cr}/H_c) 1. theoretical curves and tests using titanomagnetite data. J. Geophys. Res.: Solid Earth (1978–2012) 107, EPM-4.
Elishewitz, B., 1963. A new interpretation of the structure of the Miaoli area in the light of the décollement tectonics of northwest Taiwan. Petrol. Geol. Taiwan 2, 21–45.
Elmore, R.D., Foucher, J.L.E., Evans, M., Lewchuk, M., Cox, E., 2006. Remagnetization of the Tonoloway formation and the Helderberg group in the Central Appalachians: testing the origin of syntilting magnetizations. Geophys. J. Int. 166, 1062–1076.
Elmore, R.D., Kelley, J., Evans, M., Lewchuk, M.T., 2001. Remagnetization and orogenic fluids: testing the hypothesis in the Central Appalachians. Geophys. J. Int. 144, 568–576.
Faure, M., Chia-Yu, L., Hao-Tsu, C., 1991. Ductile deformation and miocene nappe-stacking in Taiwan related to motion of the Philippine Sea Plate. Tectonophysics 198, 95–105.
Faure, M., Monié, P., Fabbri, O., 1988. Microtectonics and ^{39}Ar-^{40}Ar dating of high pressure metamorphic rocks of the South Ryukyu Arc and their bearings on the pre-Eocene geodynamic evolution of eastern Asia. Tectonophysics 156, 133–143.
Fisher, R., 1953. Dispersion on a sphere. Proc. Roy. Soc. Lond. Ser. A. Math. Phys. Sci. 217, 295–305.
Gradstein, F.M., Ogg, G., Schmitz, M., 2012. The Geologic Time Scale 2012 2-Volume Set. Elsevier.
Halls, H., 1978. The use of converging remagnetization circles in palaeomagnetism. Phys. Earth Planet. Inter. 16, 1–11. http://dx.doi.org/10.1016/0031-9201(78)90095-X.
Ho, C., 1986. A synthesis of the geologic evolution of Taiwan. Tectonophysics 125, 1–16.
Hong, E., 1988. The sedimentary environments of the Miocene-Lower Pliocene series in Northwestern Foothills of Taiwan based on lithofacies and Ichnofacies analyses. Ph. D. thesis. National Taiwan University. In Chinese, 114p.
Horng, C.S., 2014. Age of the Tananwan formation in northern Taiwan: a reexamination of the magnetostratigraphy and calcareous nannofossil biostratigraphy. Terres. Atmosph. Ocean. Sci. 25, 137–147.
Hsiao, L., Lin, K., Huang, S., Teng, L., 1999. Structural characteristics of the southern Taiwan-Sinzi folded zone. Petrol. Geol. Taiwan 32, 133–153 In Chinese.
Hsu, I.C., Kienzle, J., Scharon, L., Sun, S., 1966. Paleomagnetic investigation of Taiwan igneous rocks. Bull. Geol. Surv. Taiwan 17, 27–81.
Hsu, Y.J., Yu, S.B., Simons, M., Kuo, L.C., Chen, H.Y., 2009. Interseismic crustal deformation in the Taiwan plate boundary zone revealed by GPS observations, seismicity, and earthquake focal mechanisms. Tectonophysics 479, 4–18.
Hu, J.C., Yu, S.B., Chu, H.T., Angelier, J., 2002. Transition tectonics of northern Taiwan induced by convergence and trench retreat. Geol. Soc. Am. Spec. Papers 147–160.
Huang, C.Y., Wu, W.Y., Chang, C.P., Tsao, S., Yuan, P.B., Lin, C.W., Xia, K.Y., 1997. Tectonic evolution of accretionary prism in the arc-continent collision terrane of Taiwan. Tectonophysics 281, 31–51. http://dx.doi.org/10.1016/S0040-1951(97)00157-1.
Hung, J.H., Wiltschko, D., 1993. Structure and kinematics of arcuate thrust faults in the Miaoli-Cholan area of western Taiwan. Petrol. Geol. Taiwan 28, 59–96.
Juan, V.C., 1975. Tectonic evolution of Taiwan. Tectonophysics 26, 197–212.
Kang, C.C., Chang, C.P., Siame, L., Lee, J.C., 2015. Present-day surface deformation and tectonic insights of the extensional Ilan Plain, NE Taiwan. J. Asian Earth Sci. 105, 408–417.
Kirschvink, J., 1980. The least-squares line and plane and the analysis of palaeomagnetic data. Geophys. J. Int. 62, 699–718.
Kizaki, K., 1986. Geology and tectonics of the Ryukyu Islands. Tectonophysics 125, 193–207.
Lallemand, S., 2014. Strain modes within the forearc, arc and back-arc domains in the Izu (Japan) and Taiwan arc-continent collisional settings. J. Asian Earth Sci. 86, 1–11.
Lallemand, S., Font, Y., Bijwaard, H., Kao, H., 2001. New insights on 3-D plates interaction near Taiwan from tomography and tectonic implications. Tectonophysics 335, 229–253.
Lallemand, S., Liu, C.S., 1998. Geodynamic implications of present-day kinematics in the southern Ryukyus. J. Geol. Soc. China 41, 551–564.
Lallemand, S.E., Liu, C.S., 1997. Swath bathymetry reveals active arc-continent collision near Taiwan. Eos Trans. Am. Geophys. Union 78, 173–175.
Lallemand, S.E., Liu, C.S., Font, Y., 1997. A tear fault boundary between the Taiwan orogen and the Ryukyu subduction zone. Tectonophysics 274, 171–190.
Lee, C., Wang, Y., 1988. Quaternary stress changes in northern Taiwan and their tectonic significance. In: Proceedings of the Geological Society of China, pp. 154–168.
Lee, J.C., Angelier, J., Chu, H.T., 1997. Polyphase history and kinematics of a complex major fault zone in the northern Taiwan mountain belt: the Lishan fault. Tectonophysics 274, 97–115.
Lee, T.Q., Jacques, A., Hao-Tsu, C., Franoise, B., 1991. Rotations in the northeastern collision belt of Taiwan: preliminary results from paleomagnetism. Tectonophysics 199, 109–120. http://dx.doi.org/10.1016/0040-1951(91)90121-8.
Lee, T.Q., Lee, J.C., Chu, H.T., Lu, C.Y., Hu, J.C., 1998. Paleomagnetic study in a folded zone of Hsuehshan range, northeastern coast of Taiwan. Terrest. Atmosph. Ocean. Sci. 9, 643–654.
Lee, Y.H., Byrne, T., Wang, W.H., Lo, W., Rau, R.J., Lu, H.Y., 2015. Simultaneous mountain building in the Taiwan orogenic belt. Geology 43, 451–454.
Lin, A., Watts, A., Hesselbo, S., 2003. Cenozoic stratigraphy and subsidence history of the South China Sea margin in the Taiwan region. Basin Res. 15, 453–478.
Lowrie, W., 1990. Identification of ferromagnetic minerals in a rock by coercivity and unblocking temperature properties. Geophys. Res. Lett. 17, 159–162.
Lu, C., Hsu, K., 1992. Tectonic evolution of the Taiwan mountain belt. Petrol. Geol. Taiwan 27, 21–46.
Lu, C.Y., Angelier, J., Chu, H.T., Lee, J.C., 1995. Contractional, transcurrent, rotational and extensional tectonics: examples from northern Taiwan. Tectonophysics 246, 129–146.
Lu, C.Y., Malavieille, J., 1994. Oblique convergence, indentation and rotation tectonics in the Taiwan mountain belt: insights from experimental modelling. Earth Planet. Sci. Lett. 121, 477–494.
Lue, Y.T., Lee, T.Q., Wang, Y., 1995. Paleomagnetic study on the collision-related bending of the fold-thrust belt, northern Taiwan. J. Geol. Soc. China 38, 215–227.
Macedo, J., Marshak, S., 1999. Controls on the geometry of fold-thrust belt salients. Geol. Soc. Am. Bull. 111, 1808–1822.
Malavieille, J., Lallemand, S.E., Dominguez, S., Deschamps, A., Lu, C.Y., Liu, C.S., Schnurle, P., Crew, A., 2002. Arc-continent collision in Taiwan: new marine observations and tectonic evolution. Geol. Soc. Am. Spec. Papers 187–211.
Marshak, S., 2004. Salients, recesses, arcs, oroclines, and syntaxes a review of ideas concerning the formation of map-view curves in fold-thrust belts. In: Thrust Tectonics and Hydrocarbon Systems, AAPG Special Volumes, pp. 131–156.
McFadden, P., Jones, D., 1981. The fold test in paleomagnetism. Geophys. J. Roy. Astron. Soc. 67, 53–58.
McFadden, P., McElhinny, M., 1988. The combined analysis of remagnetization circles and direct observations in palaeomagnetism. Earth Planet. Sci. Lett. 87, 161–172.
Miki, M., 1995. Two-phase opening model for the Okinawa Trough inferred from paleomagnetic study of the Ryukyu Arc. J. Geophys. Res.: Solid Earth (1978–2012) 100, 8169–8184.
Miki, M., Furukawa, M., Otofuji, Y.i., Tsao, S., Huang, T., 1993. Palaeomagnetism and K-Ar ages of Neogene rocks of northern Taiwan: tectonics of the arc junction of Ryukyu and Luzon arcs. Geophys. J. Int. 114, 225–233.
Miki, M., Matsuda, T., Otofuji, Y., 1990. Opening mode of the Okinawa Trough: paleomagnetic evidence from the South Ryukyu Arc. Tectonophysics 175, 335–347.
Mirakian, D.C., Crespi, J.M., Byrne, T.B., Huang, C., Ouimet, W.B., Lewis, J.C., 2013. Tectonic implications of nonparallel topographic and structural curvature in the higher elevations of an active collision zone, Taiwan. Lithosphere 5, 49–66.
Miser, H.D., 1932. Structure of the Ouachita mountains of Oklahoma and Arkansas. Bull. Oklahoma Geol. Survey 50, 30.
Nagel, S., Castelltort, S., Wetzel, A., Willett, S.D., Mouthereau, F., Lin, A.T., 2013. Sedimentology and foreland basin paleogeography during Taiwan arc continent collision. J. Asian Earth Sci. 62, 180–204.
Nakamura, M., 2004. Crustal deformation in the central and southern Ryukyu arc estimated from GPS data. Earth Planet. Sci. Lett. 217, 389–398.
Namson, J., 1984. Structure of the western foothills belt, Miaoli-Hsinchu area, Taiwan: (III) northern part. Petrol. Geol. Taiwan 20, 35–55.
Pan, Y., Zhu, R., Banerjee, S.K., Gill, J., Williams, Q., 2000. Rock magnetic properties related to thermal treatment of siderite: behavior and interpretation. J. Geophys. Res.: Solid Earth (1978–2012) 105, 783–794.
Pueyo, E.L., Cifelli, F., Sussman, A.J., Oliva-Urcia, B., 2016. Paleomagnetism in Fold and Thrust Belts: New Perspectives, vol. 42 Geological Society, London. http://dx.doi.org/10.1144/SP425.13. Special Publications.
Rau, R.J., Ching, K.E., Hu, J.C., Lee, J.C., 2008. Crustal deformation and block kinematics in transition from collision to subduction: global positioning system measurements in northern Taiwan, 1995–2005. J. Geophys. Res.: Solid Earth 113.
Schwartz, S.Y., Van der Voo, R., 1983. Paleomagnetic evaluation of the orocline hypothesis in the central and southern Appalachians. Geophys. Res. Lett. 10, 505–508.
Shinjo, R., Chung, S.L., Kato, Y., Kimura, M., 1999. Geochemical and Sr-Nd isotopic characteristics of volcanic rocks from the Okinawa Trough and Ryukyu Arc: implications for the evolution of a young, intracontinental back arc basin. J. Geophys. Res.: Solid Earth (1978–2012) 104, 10591–10608.
Shinjo, R., Kato, Y., 2000. Geochemical constraints on the origin of bimodal magmatism at the Okinawa Trough, an incipient back-arc basin. Lithos 54, 117–137.
Shipunov, S.V., 1997. Synfolding magnetization: detection, testing and geological applications. Geophys. J. Int. 130, 405–410.
Sibuet, J.C., Letouzey, J., Barbier, F., Charvet, J., Foucher, J.P., Hilde, T.W., Kimura, M., Chiao, L.Y., Marsset, B., Muller, C., et al., 1987. Back arc extension in the Okinawa Trough. J. Geophys. Res.: Solid Earth (1978–2012) 92, 14041–14063.
Simoes, M., Avouac, J.P., 2006. Investigating the kinematics of mountain building in Taiwan from the spatiotemporal evolution of the foreland basin and western foothills.

J. Geophys. Res.: Solid Earth (1978–2012), 111.
Simoes, M., Beyssac, O., Chen, Y.G., 2012. Late Cenozoic metamorphism and mountain building in Taiwan: a review. J. Asian Earth Sci. 46, 92–119.
Sonnette, L., 2012. Etude structurale et paléomagnétique de la courbure des systèmes plissés et chevauchants des arcs de Nice, de Castellane et du Nord-Est de Taiwan. Ph. D. thesis. Université Nice Sophia Antipolis.
Suppe, J., 1980. A retrodeformable cross section of northern Taiwan. Proc. Geol. Soc. Chinal 23, 46–55.
Suppe, J., 1981. Mechanics of mountain building and metamorphism in Taiwan. Mem. Geol. Soc. China 4, 67–89.
Suppe, J., 1983. Geometry and kinematics of fault-bend folding. Am. J. Sci. 283, 684–721.
Suppe, J., 1984. Kinematics of arc-continent collision, flipping of subduction, and back-arc spreading near Taiwan. Mem. Geol. Soc. China 6, 21–33.
Suppe, J., 1986. Reactivated normal faults in the western Taiwan fold-and-thrust belt. Mem. Geol. Soc. China 7, 187–200.
Sussman, A.J., Pueyo, E.L., Chase, C.G., Mitra, G., Weil, A.B., 2012. The impact of vertical-axis rotations on shortening estimates. Lithosphere 4, 383–394.
Teng, L.S., 1990. Geotectonic evolution of late Cenozoic arc-continent collision in Taiwan. Tectonophysics 183, 57–76.
Teng, L.S., Lee, C., Tsai, Y., Hsiao, L.Y., 2000. Slab breakoff as a mechanism for flipping of subduction polarity in Taiwan. Geology 28, 155–158.
Teng, L.S., Lee, C.T., 1996. Geodynamic appraisal of seismogenic faults in northeast Taiwan. Proc. Geol. Soc. China 39, 125–142.
Teng, L.S., Wang, Y., Tang, C., Huang, C., Huang, T., Yu, M., Ke, A., 1991. Tectonic aspects of the Paleogene depositional basin of northern Taiwan. In: Proceedings of the Geological Society of China, pp. 313–336.
Ustaszewski, K., Wu, Y.M., Suppe, J., Huang, H.H., Chang, C.H., Carena, S., 2012. Crust-mantle boundaries in the Taiwan-Luzon arc-continent collision system determined from local earthquake tomography and 1D models: Implications for the mode of subduction polarity reversal. Tectonophysics 578, 31–49.
Verwey, E., 1939. Electronic conduction of magnetite (Fe_3O_4) and its transition point at low temperatures. Nature 144, 327–328.
Van der Voo, R., 2004. Paleomagnetism, oroclines, and growth of the continental crust. GSa Today 14, 4–9.
Wageman, J.M., Hilde, T.W., Emery, K., 1970. Structural framework of East China Sea and Yellow Sea. AAPG Bull. 54, 1611–1643.
Wang, K.L., Chung, S.L., Chen, C.H., Shinjo, R., Yang, T.F., Chen, C.H., 1999. Post-collisional magmatism around northern Taiwan and its relation with opening of the Okinawa Trough. Tectonophysics 308, 363–376.
Wang, K.L., Chung, S.L., O'reilly, S.Y., Sun, S.S., Shinjo, R., Chen, C.H., 2004. Geochemical constraints for the genesis of post-collisional magmatism and the geodynamic evolution of the northern Taiwan region. J. Petrol. 45, 975–1011.
Weil, A.B., Sussman, A.J., 2004. Classifying curved orogens based on timing relationships between structural development and vertical-axis rotations. Geol. Soc. Am. Spec. Papers 383, 1–15.
Yang, H.Y., 1986. The deuteric alteration and the spilitic degradation of Kungkuan basaltic rocks in northern Taiwan. Acta Geol. Taiwanica 179–210.
Yeh, Y.H., Eric, B., Lin, C.H., Jacques, A., 1991. Stress tensor analysis in the Taiwan area from focal mechanisms of earthquakes. Tectonophysics 200, 267–280.
Yonkee, A., Weil, A.B., 2010. Quantifying vertical axis rotation in curved orogens: correlating multiple data sets with a refined weighted least squares strike test. Tectonics 29.
Yoshiwara, S., 1901. Geological Structure of the Riukiu (Loochoo) Curve, and Its Relation to the Northern Part of Formosa. College of Science, vol. XVI Imperial University.
Yu, S.B., Chen, H.Y., Kuo, L.C., 1997. Velocity field of GPS stations in the Taiwan area. Tectonophysics 274, 41–59. http://dx.doi.org/10.1016/S0040-1951(96)00297-1.
Yue, L.F., Suppe, J., Hung, J.H., 2005. Structural geology of a classic thrust belt earthquake: the 1999 Chi-Chi earthquake Taiwan (M_w = 76). J. Struct. Geol. 27, 2058–2083.
Zheng, Z., Zhao, X., Horng, C.S., 2010. A new high-precision furnace for paleomagnetic and paleointensity studies: Minimizing magnetic noise generated by heater currents inside traditional thermal demagnetizers. Geochem. Geophys. Geosyst. 11, n/a–n/a. http://dx.doi.org/10.1029/2010GC003100.